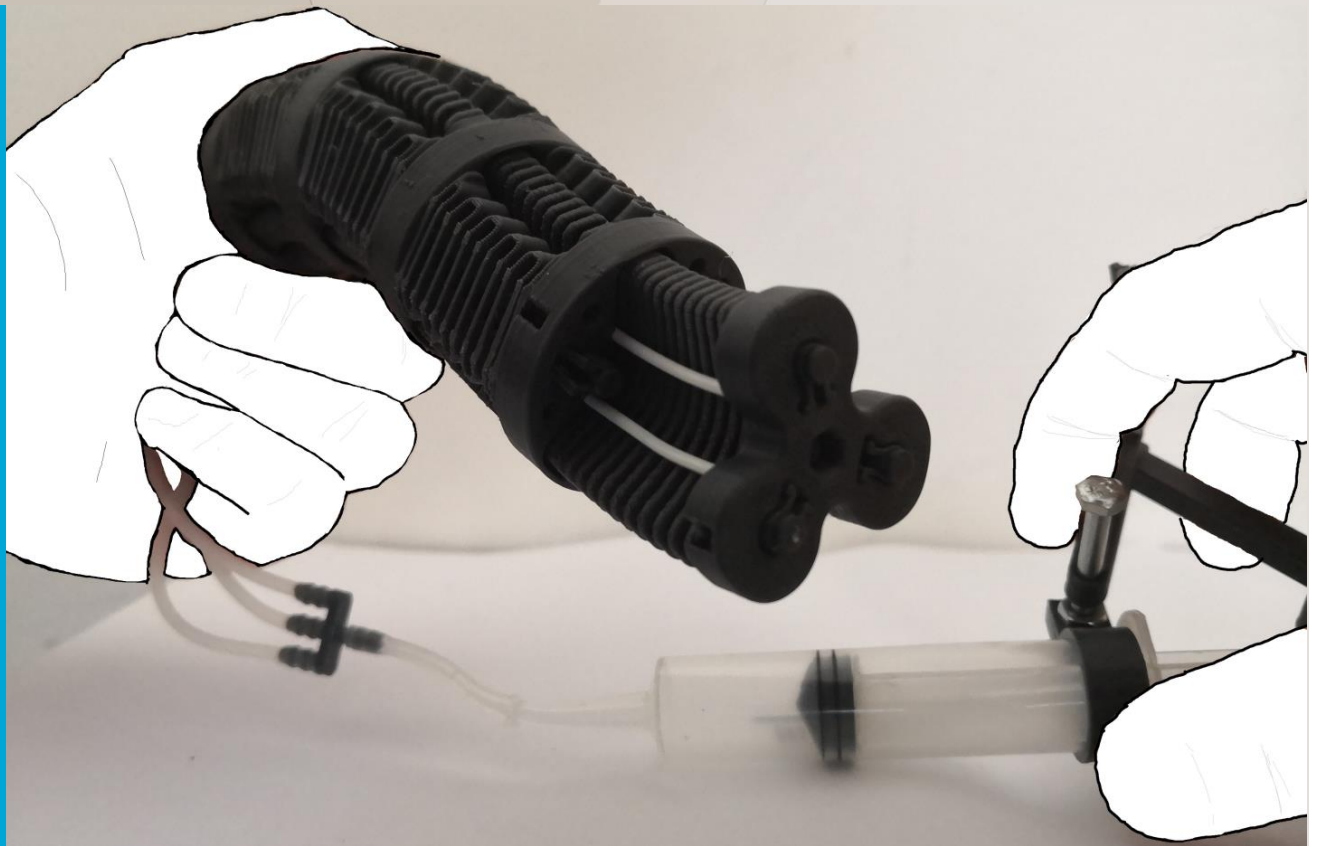


Alternating Follow-the-Leader Medical Device with Pneumatically Actuated Shape Locks

F. Semih Yikilmaz

Delft University of Technology



Alternating Follow-the-Leader Medical Device with Pneumatically Actuated Shape Locks

By

F. Semih Yikilmaz

in partial fulfillment of the requirements for the degree of

Master of Science
in Mechanical Engineering

at the Delft University of Technology,
to be defended publicly on Monday May 17th 2021 at 14:00.

Student number:	4373634
Supervisors:	Prof. dr. ir. P. Breedveld MSc C. Culmone Ir. F. Trauzettel
Thesis committee:	Prof. dr. ir. P. Breedveld, TU Delft Dr. J. J. van den Dobbelsteen, TU Delft

This thesis is confidential and cannot be made public until May 17, 2021

An electronic version of this thesis is available at <http://repository.tudelft.nl/>.

Preface

More than a year ago I found myself struggling to find a thesis as many professors were occupied with up to 20 students to supervise. After looking for some open projects I e-mailed Juan Cuellar who helped me find a project as he was leaving soon. He forwarded me to Fabian Trauzettel and Costanza Culmone who had some interesting projects to be realized. As Paul Breedveld agreed I could finally start researching Follow-the-Leader medical devices to ultimately design my own. I enjoyed analyzing and categorizing Follow-the-Leader medical devices and was very excited when it was decided to publish my literature study.

Unfortunately, shortly after, a bunch of social interaction restrictions were pushed by the Dutch government to prevent the spread of Covid-19. This pandemic greatly interrupted the possibility to have progressive meetings with drawings, prototypes, and simple face-to-face contact. By taking pictures and videos I tried to visualize the progress of my thesis, which worked out sufficiently. The biggest impact was on the production of my prototype. I realized in March 2020 that it would be best if I purchased my own 3D printer to effectively produce the prototype from home. With my budget, the best printer I could find was the Creality Ender 3. It took much time to learn about the printer before I could confidently produce anything. From bed leveling, to surface adhesion, material temperature, tolerances, and much more, I was a long way from printing a prototype. However, the experience has thought me a lot in the end and I always wanted a 3D printer to begin with.

I want to thank Paul Breedveld for his advice, knowledge, and the opportunity to dive into the world of novel medical devices on a high level. I also want to thank Costanza Culmone and Fabian Trauzettel for their advice, revision, knowledge, experience, and flexibility during this pandemic. The productive online meetings felt more like pleasant chatter. I want to thank my parents, my sister, and friends who supported me in this process with multiple lockdowns and provided an exhaust during a time where everything is closed and restricted.

*F. Semih Yikilmaz
Gouda, April 2021*

CONTENTS

I	Introduction	1
I-A	Background in Minimally Invasive Surgery	1
I-B	Follow-the-Leader motion	1
	I-B1 State-of-the-Art	1
	I-B2 Alternating devices	2
I-C	Design motivation	2
I-D	Goal	4
I-E	Structure	4
II	Conceptualization	4
II-A	Requirements	4
II-B	Morphological overview	4
	II-B1 Design aspects and solutions	5
	II-B2 Assessment of solutions	5
	II-B3 Compatibility of solutions	6
II-C	Design concept	6
III	3D Design	8
III-A	Inner-shaft design	8
	III-A1 Segment disk design	8
	III-A2 Segment joint design	9
	III-A3 End-effector disk and stand design	10
III-B	Outer-shaft design	10
	III-B1 Segment disk design	10
	III-B2 Segment joint design	11
	III-B3 End-effector disk and stand design	11
IV	Prototyping and assembly	11
V	Testing and results	12
V-A	Operating force test	12
V-B	Precision test	13
	V-B1 Tip bending test	13
	V-B2 FTL advancement test	13
	V-B3 FTL retraction test	14
VI	Discussion	14
VI-A	Evaluation and improvements	14
VI-B	Design alternatives	14
	VI-B1 Tube arrangement	14
	VI-B2 Locking mechanism	15
VI-C	Future work	18
VII	Conclusion	18
	References	19
	Appendix	21
A	Engineering drawings	21
B	Prototype pictures	41
C	Part replacement demonstration	44

Abstract—Developments in minimally invasive surgery such as natural orifice transluminal endoscopic surgery and single port laparoscopic surgery have pushed medical devices to be higher articulated and more dexterous. These surgery methods have proven to greatly decrease bleeding, scar tissue, hospital time, and cost. The procedures involve the navigation of flexible instruments through tortuous anatomical pathways. To reduce chances of tissue damage it is desired to reduce the interaction with anatomical structures during the trajectory. To realize this aspect a so-called Follow-the-Leader (FTL) motion has been adapted as a design feature for medical devices. This motion allows for the shaft of the instrument to conform to the shape taken by its end-effector without relying on anatomical reaction forces. One strategy to achieve FTL motion is the so-called alternating advancement where two shafts subsequently switch from flexible to stiff in order to conserve the configuration of the shaft. These devices have been shown to possess relatively many degrees of freedom for a small number of actuators which can greatly reduce the cost of the device. A state-of-the-art analysis has shown that, despite the kinetic advantages, there are no alternating FTL devices that use pneumatically actuated shape locks to constrain the flexibility of the shaft. In this work an alternating FTL medical device with pneumatically actuated shape locks was designed, produced, and tested. The device has a diameter of 40 mm and nine degrees of freedom. The total bending angle is 90 degrees with a bending radius of 85 mm. The device leaves room for improvement but does show that two concentric shafts can be shape locked pneumatically to perform an alternating FTL motion.

I. INTRODUCTION

A. Background in Minimally Invasive Surgery

With conventional open surgery, the area of intervention is exposed with a large incision to have sufficient reach. These incisions are mostly about 5.5 cm but can be up to 16 cm and lead to many undesirable consequences such as long hospital time, large scar tissue, pain, bleeding, and the chance of infection [1]. In recent years, minimally invasive surgery (MIS), a surgical method that reduces the incision size, has been adopted. MIS has proven to lead to a sooner recovery of the patient, less scar tissue, less pain, less use of anesthesia, and a smaller chance of infection [2]–[4]. MIS is performed by making small strategical incisions around the anatomical target which is then reached with rigid slender instruments from various sides, Figure 1-A [5]. A more novel practice in MIS is to limit the incisions to one, thus greatly increasing the advantages of MIS. The so-called single-port laparoscopy (SPL) aims to reach anatomical targets from one entry point, Figure 1-B [6], [7]. A different method is to partially advance without any incisions by the so-called natural orifice transluminal endoscopic surgery (NOTES) [8]–[11]. These procedures approach anatomical targets, for example, by traversing through the gastrointestinal system, Figure 1-C. Both SPL and NOTES require far more elaborate and higher articulated devices compared to the instruments used in traditional MIS [12], [13]. In order to have the same reach with only one port or orifice the devices would need to be able to circumnavigate certain anatomical obstacles.

Furthermore, the gastrointestinal system contains tortuous lumen which cannot be approached with rigid instruments. Often flexible and steerable devices are used to conform to the shape of the anatomical pathway. Moreover, due to the passive flexibility of the flexible instruments, the gastrointestinal lumen exerts undesired reaction forces to guide instruments causing possible tissue damage [14].

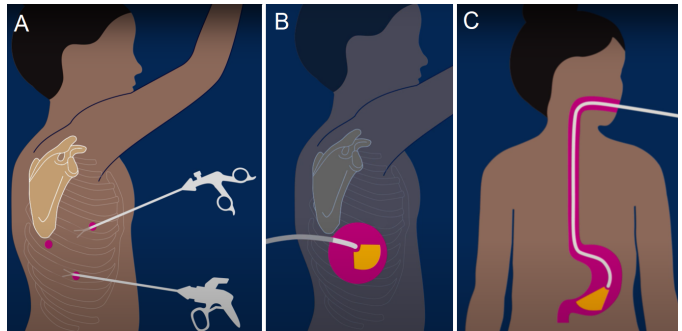


Fig. 1: **Schematic representation of various MIS procedures.** (A) Traditional MIS. (B) SPL. (C) Flexible endoscopy. Adapted from [5].

B. Follow-the-Leader motion

Following the demand for instruments that can adequately perform novel MIS procedures, a so-called Follow-the-Leader (FTL) motion has been a design feature for medical devices [15]. This motion enables a snake-like advancement where the shape of the snake’s body conforms to the path taken by its head as illustrated in Figure 2. In medical application, an FTL device can be defined as: “An instrument that operates in a so-called follow-the-leader manner where the body conforms approximately to the path taken by its end-effector without relying on anatomical interaction forces” [16]. The distal end-effector assumes a leader role where relative proximal parts of the device assume their leader’s previous orientation and thus follow the leader. In doing so the device progresses independently from the anatomical environment by carrying its weight in any configuration. By performing FTL motion, medical devices can circumnavigate anatomy and avoid applying forces to lumen or tissue.

1) *State-of-the-Art*: In general, medical devices consist of a control unit outside the body (e.g. handle or joystick) that operates a shaft that enters the body. Shafts of FTL devices are often segmented to have more Degrees of Freedom (DOF) to control the configuration of the shaft. Many proposed FTL medical devices control each segment of the shaft independently to ensure that the shape conforms to the path taken by the leader/end-effector [17], [18]. Therefore, the devices need an actuator for each degree of freedom. A control algorithm shifts the segments to their desired orientation in an effort to maintain an FTL motion. The actuators are sometimes embedded inside the segment which increases

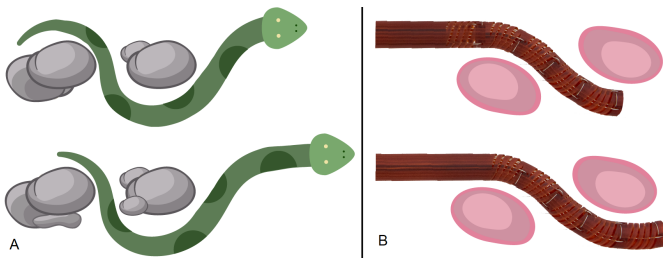


Fig. 2: **Schematic representation of FTL motion analogy.** (A) A snake avoiding rocks on its path as its body follows the path taken by its head. (B) A medical instrument avoiding anatomical obstacles as the shaft conforms to the path taken by the end-effector. Ultimately the target is reached without exerting any forces on the anatomy. [15]

the diameter of the shaft that enters the body [19], [20]. These devices have a likelihood of being incompatible in an electromagnetic (EM) environment as needed during real-time imaging such as magnetic resonance imaging (MRI). Moreover, the use of actuators in parts that enter the body is discouraging from a safety perspective since these actuators draw potentially lethal currents and heat up [21], [22].

Conversely, most devices control the segments with actuators located outside the body by orientating the segments in the shaft with cables [23], [24]. The control modules of such devices are often bulky and have a motor for each DOF. A software algorithm determines the desired orientation of each segment depending on the shaft propagation by applying virtual constraints to their movement. Whilst greatly improving the dexterity of medical devices compared to conventional devices, the cost increases significantly [25], [26]. Moreover, the reliability of the devices decreases because there is a dependence on a large number of actuators that all carry a risk of failure [27], [28].

Other popular solutions for FTL movement are the so-called concentric tube devices [29]–[31]. These devices consist of concentrically telescoping pre-curved tubes. The tubes conform to their shape of least potential energy by elastic relaxation and interaction when translated and rotated respectively to each other. The tubes pose physical constraints to each other related to the hardware of the device to maintain the desired configuration from an FTL perspective. This supplies an inherent steering mechanism that is dependent on the propagation, thus allowing the design and manufacturing of FTL devices with the smallest diameters [15]. However, a tube pair can only possess two DOFs and therefore the number of DOF per actuator is similar to other FTL devices. Moreover, the imposed plastic deformation on these pre-curved tubes is highly dependent on the type of procedure and the shape of its related anatomical pathways. This means that for each anatomical pathway a different device has to be produced [32]–[34]. If the pathway for a certain procedure is consistent this might not be a problem. However, sometimes more adaptive

and universal devices are required as certain diseases change physical anatomy (e.g. brain tumor) [35].

2) *Alternating devices*: A different strategy in achieving FTL motion is used by the so-called alternating devices [36], [37]. These devices consist of two shafts that have adjustable flexibility. While one shaft is assuming a stiff state, the other shaft advances in a flexible state with physical path guidance from the stiff shaft. By alternating the stiffness of the two shafts and switching the advancing motion, the shape of the path taken by the end-effector is conserved. Figure 3 shows such an alternating device called HARP which is commercially available as Flex® Robotic System by Medrobotics® [38]. The HARP applies a normal force with cables to compress its segments. This compression causes friction between segment contact surfaces that holds the shape of the shaft. Alternating systems show the highest degrees of freedom while keeping the number of actuators at a minimum [15]. Only the end-effector of the shaft has to be steered since the orientation and advancement of the follower segments are passively guided by a physical track. This actuation is currently mostly done from outside the body and therefore possesses the size, safety, compatibility, and reliability advantages mentioned before. Other alternating devices use actuators inside the body to lock the shape of the shaft [39], [40]. This increases the diameter and loses the benefits of actuating all sub-functions (e.g. steering, advancing, and locking) of the device with actuators located outside the body.

C. Design motivation

A state-of-the-art analysis has shown the advantages of alternating devices and an absence of pneumatically actuated FTL medical devices [15]. Furthermore, the use of geometry-based shape locks as a physical constraint mechanism rather than friction-based locks is scarce in FTL medical devices. A geometry-based shape lock means that a geometry that initially has a DOF loses its DOF by interlocking with another geometry.

Medical devices often use friction-based stiffening mechanisms such as granular, layer, and wire jamming [41]–[43]. An important difference is that friction-based locking depends on the normal force applied to the locking surface whereas geometry-based locking is independent of the force of the locking actuation. For friction-based systems, a higher normal force will increase the friction forces. Depending on the shape of the device, these surfaces can be orientated differently leading to different local locking forces [41]. A geometry-based shape lock only requires a force to initiate the movement of the geometries to interlock with each other. Once settled, the stiffening of the shaft should be globally similar and independent of the applied force. The disadvantage is that the geometry can only settle in a discrete number of positions whereas friction forces apply across the whole surface. The size of the

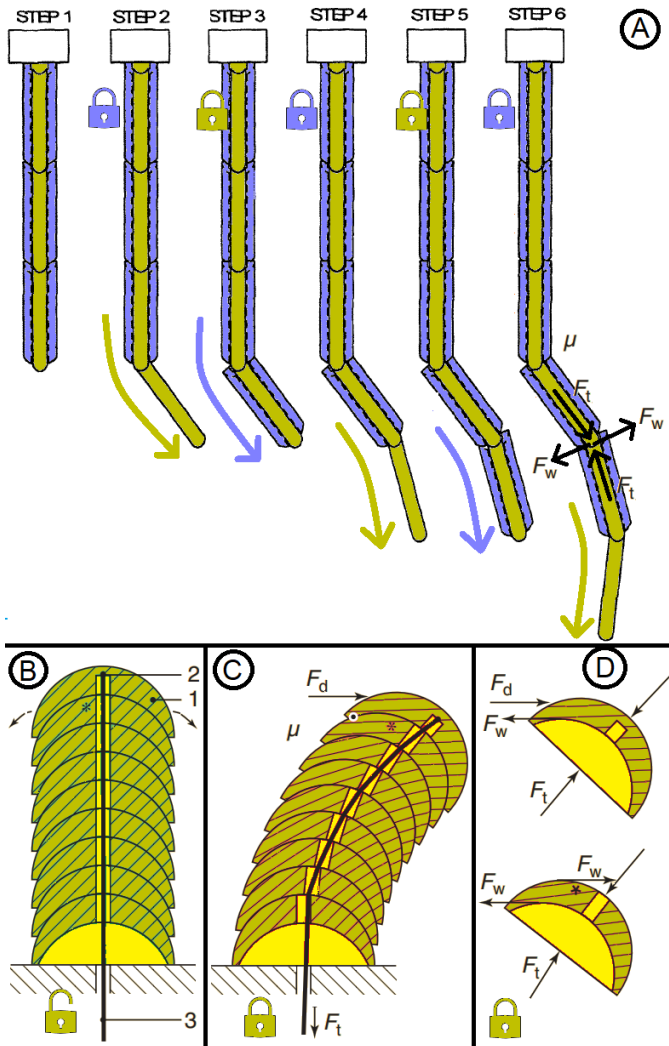


Fig. 3: **Schematic drawings of the HARP.** (A) A patent drawing of the HARP depicting an alternating FTL motion. Adapted from [36]. From Step 1 to Step 2 the outer-shaft segments (blue) are locked and constrain the propagating motion of the inner-shaft segments (yellow). From step 2 to step 3 the inner-shaft segments are locked and constrain the catch-up motion of the unlocked outer-shaft segments. By alternating the stiffness and propagation of both shafts the shape of the traversed path is conserved. (B) A schematic representation of the HARP friction lock working principle. Adapted from [41]. The segments (1) are shaped like ball-socket joints and thus are free to rotate. A cable (3) is attached to the end (2) of the shaft (C) When this cable is in tension (F_t) the segments with a coefficient of friction μ are pressed against each other. (D) If external forces (F_d) are applied to the shaft the friction forces (F_w) hold the configuration of the segments.

interlocking geometry can be reduced to increase the continuity which in turn decreases its structural strength.

The curvatures in the shaft can affect the friction forces especially if the normal forces are imposed by cables as done in the HARP. Forces in cables can only assume a direction co-linear to the cable. This means that if the cable is operated from outside the body, the shaft

not only produces internal friction forces that hold the shape, but also internal forces that want to straighten the shaft. If the locking force is initiated by a pneumatically expanding tube, the forces will be equal and radial to the tube independent of the curvature of the shaft. A disadvantage of pneumatically actuated shape locks is that miniaturizing the system reduces the output force of the system since the radial forces are related to the diameter of the tube. Therefore, pneumatic actuation is especially suited to a combination with geometric shape locks, as the pneumatic force only needs to displace a locking mechanism and does not need to oppose shape-distorting forces directly. If, in any case, the pressure needs to be higher, liquids can be used instead of air. Often a saline solution is used as a safety measure with pressures that don't damage the lumen [44]. The medical device proposed by Yagi et al. shows an example of pneumatically operated shape locks, Figure 4 [45]. The shaft is flexible when the air tube is collapsed but locks the segments in their orientation when the air tube is inflated. This device has a single shaft consisting of multiple segments and cannot perform FTL behavior.

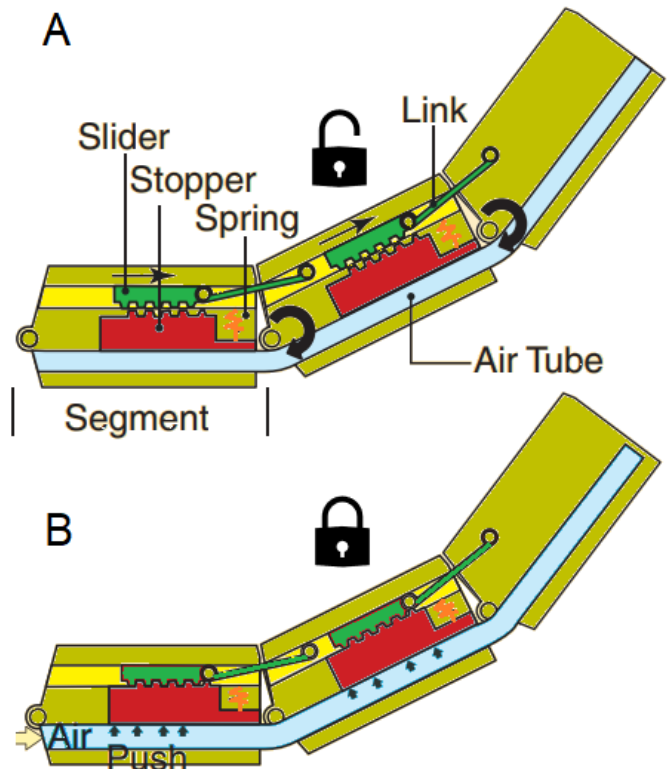


Fig. 4: **Schematic side-section view that shows the working principle of a pneumatically actuated shape lock mechanism in an endoscope.** (A) The endoscope consists of segments that are attached with revolute joints. As the shaft bends the links push or pull the sliders inside the proximal segment. (B) When the air tube inflates, shape locking stoppers will interlock their teeth with the sliders. Adapted from [45]

D. Goal

Considering the novelty and benefits of using pneumatic actuation and shape locks to achieve FTL motion in a medical device, a design for a new highly articulated probe will be made. To assess whether this device could reach medical application, a prototype will be made and tested. Ultimately, the goal of this work is to **design, produce, and test a proof of concept alternating FTL medical device with a pneumatically actuated shape locking mechanism**. Following the design motivation, the device has to possess an FTL behavior by performing an alternating motion in which pneumatically actuated shape locks apply a physical constraint to the orientation and movement of the shaft segments.

E. Structure

Leading up to the prototype, first, a design conceptualization was done in Section II. Afterward, a 3D design was made and described in Section III. The production and assembly of this design were then covered in Section IV. The testing and results of this prototype were then reported in Section V. In Section VI the results of the test were discussed and some recommendations and improvements were given in a context of fewer limitations to time and production capabilities. Furthermore, various design alternatives were proposed and discussed.

II. CONCEPTUALIZATION

A. Requirements

The device has the following requirements related to the fundamental working principle and the design motivation:

- The device has to be able to propagate and retract in an FTL manner.
- The device has to achieve FTL motion by applying the alternating strategy.
- The device has to alternate the flexibility of the shafts by applying physical constraints.
- The device has to apply physical constraints with shape locks.
- The shape locks have to be actuated by a pneumatically operating mechanism.
- The forces for the steering, propagation, and shape locking of the device have to be applied from outside the shaft.

Furthermore, the device has the following requirements related to its performance:

- The device has to operate in 3D.
- The device has to be able to form a clear C-curve and S-curve.
- The diameter cannot exceed 40 mm.

In order not to interact with the anatomical environment at any moment the device has to be able

to not only advance in an FTL manner but also retract in an FTL manner. As alternating devices allow for many DOFs with a relatively low number of actuators this was the preferred strategy to achieve FTL motion. Working towards novelty and kinetic advantages, pneumatically activated shape locks will provide a physical constraint. Having all motions and constraints actuated from outside the shaft will further prove that the device can benefit from the size, EM compatibility, reliability, and safety advantages as opposed to devices with actuators located inside the shaft. Even though the working principles of FTL devices remain similar when simplified from 3D to 2D, the design for 3D application is often much more complicated. The proof of concept prototype has to be operational in 3D to have a more direct real-world application. Furthermore, FTL motion is often demonstrated when performing C- and S-curves to follow an anatomical path or to avoid anatomical obstacles [35], [37]. Therefore, having a prototype that has the DOFs to perform these curves is desirable. To have a clear vision of these curves the minimum angle of each segment is set as 30 degrees.

Actuating the advancing motion and steering with motors can provide higher precision and speed because the sequence of the motions is programmed. Ideally, the operator only steers the leader and adjusts the advancement speed whilst the catch-up sequence is automated accordingly. These aspects are out of the scope of this work because they do not contribute to proving the concept working principle and are therefore simplified to passive manual mechanisms. The size limit of the prototype is motivated by the diameter of various devices used in robotic endoscopy which often does not exceed 20 mm [13], [46], [47]. Aware of the production limitations and the aim to merely prove a working principle, this diameter is doubled for the limit of the prototype that will be fabricated at a diameter of 40 mm. Finally, as discussed earlier, the alternating FTL devices allow for a setup where all forces are applied from outside the body. To benefit from these advantages the prototype has to prove that possibility. The specifications such as bending angle, DOFs, size, mass, precision, and operating force of the prototype proof of concept will be tested, but are not assigned as requirements due to the novelty of the design proposed.

B. Morphological overview

To systematically reach adequate design choices, the alternating system was dissected into design aspects. Only design aspects that comply with the design requirements were analyzed. Then, for each solution of a design aspect, the advantages and disadvantages were discussed. Finally, the most suitable solutions were combined to form the foundation of the design. Figure 5 shows the morphological overview of the solutions to the design aspects.

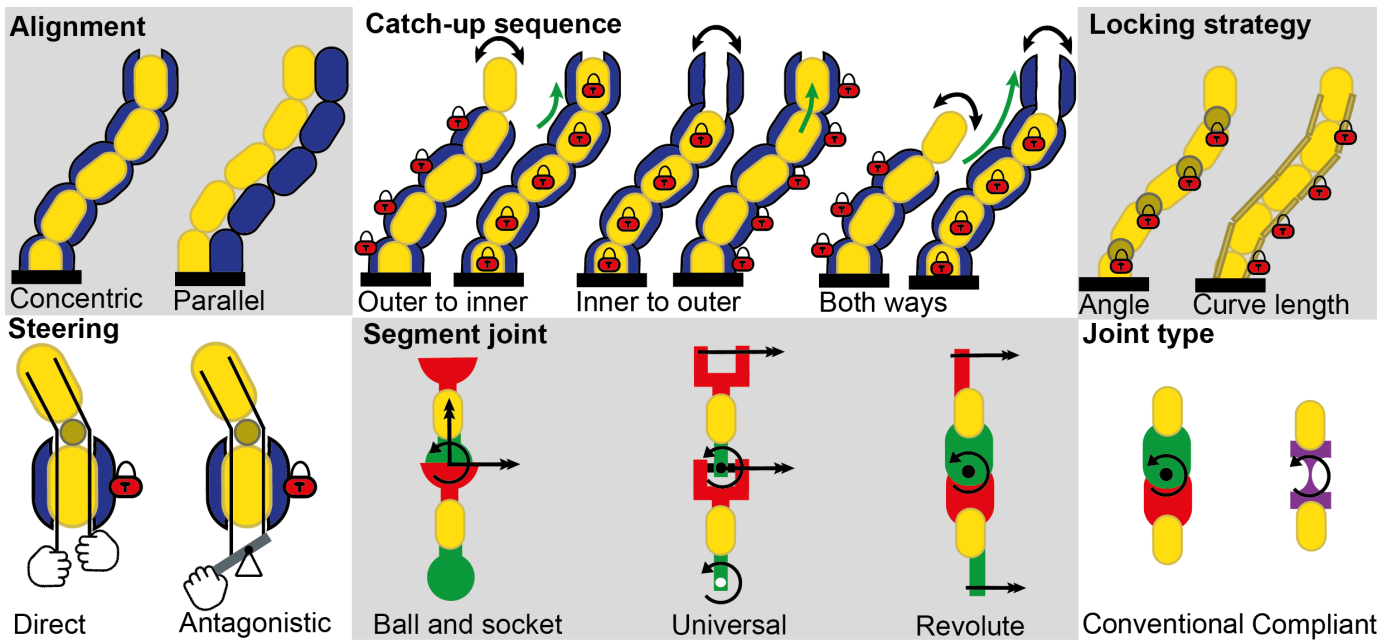


Fig. 5: **Morphological overview.** The alternating FTL system is dissected into design aspects. Alternative solutions for each design aspect are schematically shown. Segments of the inner and outer shaft are shown in yellow and blue respectively. The red locks indicate that the segments are fixed in their position and orientation.

1) *Design aspects and solutions:* The first design consideration is the **alignment** of the alternating shafts. They can be placed concentrically or parallel [48] to each other. Next, the advancement sequence of the devices can be different. Depending on the design it might be beneficial to have the inner- or outer-shaft catch-up on its counterpart, dividing the follower and leader roles of the motion. This will be called the **catch-up sequence**. Another option is to have both shafts operating as both follower and leader and subsequently catch up on each other. For the **steering**, the kinetic mechanism manipulating the orientation of the end-effector is cable-tension in which the segment changes orientation because cables pull the segment with a moment arm from its pivot point. Following the design requirements, this is a relatively conventional and feasible way of steering that allows for actuation outside the body. The cables can be operated independently or in an antagonistic setup. In antagonistic steering systems, opposing tendons in a segment are actuated simultaneously and with the same magnitude, but in opposite directions. The segments can be connected with various **segment joints** to construct a segmented shaft, such as ball-and-socket joints, universal joints, or perpendicularly stacked rotational joints. These **types of joints** can be conventional or in the form of a compliant mechanism, such as a flexible shaft or the construction of flexible beams. To lock the shaft, different **locking strategies** are available [41]. The shape of the shaft is conserved if the curvature length or the angles between segments are maintained.

2) *Assessment of solutions:* The disadvantage of a concentric **alignment** is that the outer shaft strictly has to

be larger in diameter to fit the inner shaft. Furthermore, it requires a different design for both shafts. For parallel mechanisms, two smaller shafts could potentially reduce the overall thickness in one dimension and they could be identical in design. Depending on the application a device with a non-circular cross-section might be sufficient. If the device only needs to bend in one plane this could be the case. However, a parallel alignment would require a guidance mechanism (e.g. slide or rail) that connects the two alternating shafts, which could increase the overall geometry of the cross-section. A concentric alignment inherently guides over the whole contact perimeter and the imposed advancement force is co-linear to the centerline of both shafts. A parallel alignment can only guide from one side and has a moment arm from the centerline of the guiding part to the centerline of the shaft. Finally, the radius of curvature of each parallel aligned shaft is different for each turn. In the case of the concentric alignment, the radius of curvature is the same for the center-line of both shafts however, the outer shaft will have a larger diameter and therefore its geometry will force a larger radius of curvature than the inner shaft.

For the **catch-up sequence**, it is important to note that the shafts have to be able to conform to each other's shape. Therefore, the leader shaft should be the shaft that has the least range in curvature so the follower shaft can always conform to the boundary conditions of the leader. In the case of a concentric alignment, this is the outer shaft. In the case of a parallel alignment, it depends on the direction of the turn. Since the leader shaft initiates the direction of propagation, it has to be the steerable shaft. If the catch-up sequence goes both ways,

both shafts need a steering mechanism that increases the complexity and number of actuation units of the device without gaining any DOFs. However, by assigning both shafts with a leader role in the catch-up sequence, the advancement speed might increase because double the distance is traveled for a single locking instant. Reducing the procedure time is crucial to benefit from a cost point of view [49], [50]. Therefore advancing with both shafts might be beneficial if the locking mechanism takes long to activate, settle, and/or deactivate. This is unlikely to be the case with pneumatic actuation.

For manual **steering**, it is an option to operate steering mechanisms separately or kinetically dependent. As one cable is retracted the opposite cable is released. This provides a physically similar orientation between the segment and steering module making it easier to steer the end-effector. Since the design requirement is a device functioning in 3D, the end-effector needs at least three steering cable attachment points symmetrically around the joint. Operating three cables by one person is less convenient than a single lever. The disadvantage is that the bending angle per segment is limited by the steering module because the module has to contain a joint to relate the translations. The lever cannot exceed a 90-degree angle. To solve this angle limit additional mechanisms like gears and pulleys are needed. If the steering is done with actuators, three actuators are needed regardless of the steering setup.

There are two different **strategies** to structurally **lock** the shape of a hyper-redundant or flexible shaft [41]. The first strategy is to lock the angle between segments (joint locking) and the second strategy is to lock the curve length of the shaft (curve length locking). Joint locking will have to withstand higher perturbation forces compared to curve length locking due to the moment arm increase. This aspect will affect the operating force of the device. Depending on the joint, one strategy is more convenient than the other. Ball-and-socket, universal, and revolute joints provide three, two, and one DOFs respectively. Having more DOFs per segment means that fewer segments are needed to provide the same reach. Since the segments contain rigid parts, and they add length to the shaft, more segments in series will affect the continuity of the device. However, more DOFs in a joint will reduce the reliability of an angle locking mechanism. For two geometries to interlock reliably, they must be on the same plane. If the joint operates on multiple planes, the locking geometry has to be reduced to a one-dimensional geometry to be able to interlock with its counterpart in all orientations (pitch and yaw). Therefore, ball-and-socket joints are fit for friction-based locking, as seen in the HARP device, where the lock is continuous across the whole joint surface. Furthermore, the rolling angle of a ball-and-socket joint is not desired since it disturbs the axial direction of the steering cables. A universal joint contains two joints that each operate in a single plane perpendicular to each other. This means that rows of interlocking geometry can always align with

each other when actuated by pneumatic inflation. The same principle holds for single revolute joints, but they only provide one DOF per segment.

Finally, a choice has to be made for the **type** of segment **joint**. Compliant mechanisms require the implementation of long and slender geometry that will likely increase the size of the device. Even in a proof of concept, this poses a problem since the stiffness is related to the length in the 3rd order ($k = \frac{12EI}{l^3}$). This means that scaling the length with s will change the stiffness with s^3 . If the whole geometry is scaled by s the stiffness k will scale with s ($\frac{[I]}{[l^3]} = \frac{m^4}{m^3} = m$). However, if the thickness of the compliant beams is decreased the strength of the joint will also decrease. Conversely, the predictable behavior and low hysteresis of compliant joints offer an advantage over conventional joints from a precision perspective. Since the majority of the parts will be 3D-printed it is also a motivation to implement compliant joints from a production point of view. To counter the scaling problem, more flexible material can be used for the joints.

3) *Compatibility of solutions*: It is important to note that solutions to some design aspects can limit the possibility of using solutions to other design aspects. If an angle locking strategy is preferred the use of compliant joints is not possible. The working principle of compliant joints requires the implementation of slender geometry consisting of one part that provides DOFs with elastic bending. This means that compliant joints cannot contain mechanisms to constrain the relative rotation of segments, therefore limiting the design aspect solution to conventional joints. Likewise, if a compliant joint is preferred the locking strategy is limited to curve length locking. Furthermore, if a concentric alignment is combined with compliant joints, only one solution for the catch-up sequence is applicable. Since the leader shaft initiates the direction of propagation, it has to be the steerable shaft. To form a bending curvature with a compliant joint without compressing the joint and altering its length, the compliant joint needs a so-called backbone. This backbone is a flexible rod concentric to the centerline of the shaft that allows for bending but prevents compression. Since the compliant joint in the outer shaft cannot have such a backbone in a concentric alignment only the inner shaft can be assigned the leader role.

C. Design concept

Considering the assessment of design aspect solutions the device was chosen to implement a concentric alignment with compliant joints. A concentric alignment was preferred in state-of-the-art alternating FTL devices as they provide inherent guidance and are more suitable to operate on two planes. Compliant joints enable the possibility to have two DOFs per segment with a single 3D-printed part. Constrained by the compatibility of the design aspect solutions the locking strategy was set as

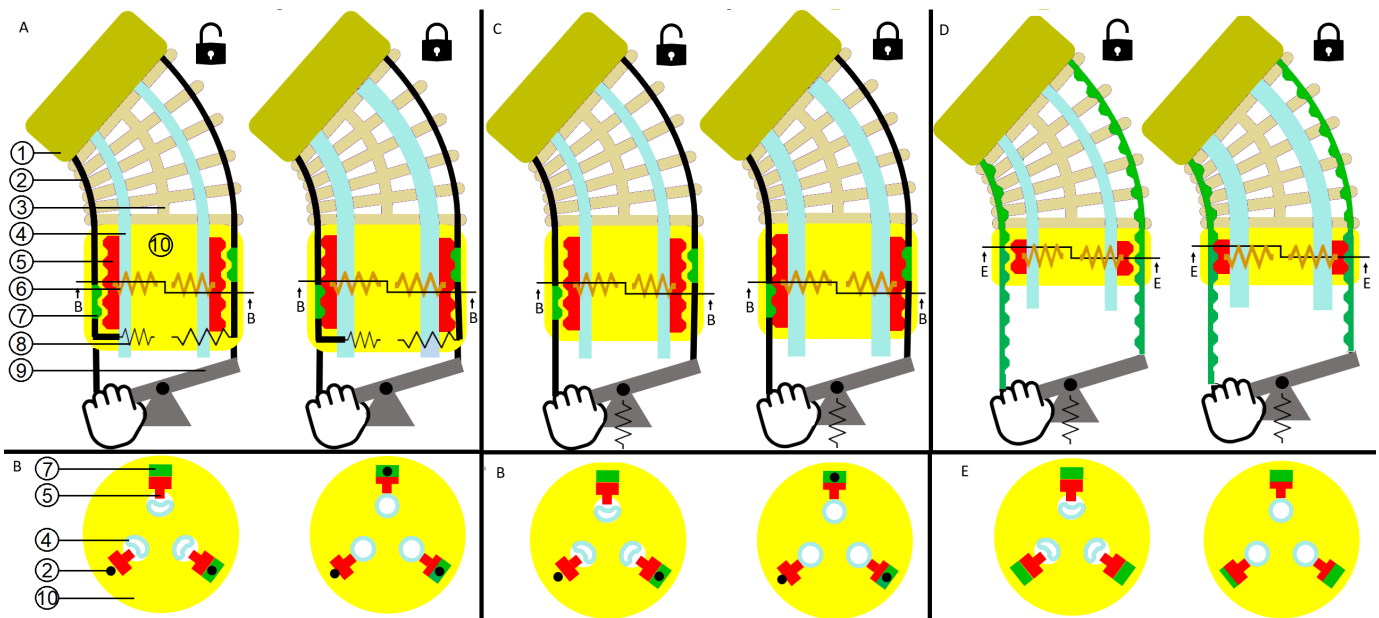


Fig. 6: **Schematic section views of the inner-shaft of the design concept.** The inner-shaft mechanism is depicted in three different versions. The basic principle is that the orientation of the rigid segments (10) and the end-effector (1) is related to the translation of the sliders (7) which can be initiated by pulling the cables (2) with the steering mechanism (9) or bending the joint (3). The sliders can be locked in their axial position with stoppers (5) which will statically determine the orientation of the segment. The stoppers have a geometry that interlocks by displacing radially towards the sliders when the air tube (4) is inflated. The springs (6) pull back the stoppers to reset the locking system when the air tubes are collapsed. (A) A side-section view of the first variation. To ensure that the cables are always in tension the cables are attached to springs (8) fixed to the rigid segment. (B) A cross-section view of the rigid segment in versions (A) and (C). As the tubes are inflated the stoppers interlock with the sliders. The black dot (2) is the cable that is connected to the distal segment or the spring within its segment. (C) A side-section view of the second variation. To keep tension in the cables all sliders are connected throughout the shaft with each other and apply constant tension to the steering mechanism. (D) A side-section view of the final version. To keep the rigid segment part small the cable and slider fused their functions. (E) A cross-section view of the rigid segment in version (D). As the tubes are inflated the stoppers interlock with the sliders that now also function as cables.

curve length locking and a catch-up sequence where the outer-shaft follows the inner-shaft. Figure 6 shows the resulting design concept. To apply curve length locking a lockable structure has to move with respect to the change of the segment orientation. To realize this, an axially moving interlocking geometry, from now on referred to as **slider**, can be constrained to axially move with the steering cables. Fixing the position of the slider will then fix the curve length in one dimension of the joint. If this is done on three points around the joint its configuration is statically determined. The radially moving interlocking geometry, from now on referred to as **stopper**, will translate when the air tubes are inflated. To be able to lock the system for every angle the stopper has to cover the entire axial length of the segment. To reset to the unlocked state a spring attached to the stopper will pull the locking teeth away from the slider when the air tube is collapsed. However, for alternating FTL mechanisms, the configuration of the segments is not only changed by steering forces but also by physical constraints imposed by the locked shaft during the advancing movement. This means that the sliders have to move as a response to the joints bending and thus compressing the cables. Since cables will buckle under this compression, it is necessary

to keep the cables under constant tension to make sure the cables want to conform to the shortest curve length between each segment.

This can be done by attaching the cables to springs that are fixed in the rigid segment parts as shown in Figure 6-A. However, these springs must not influence the orientation of the segment but merely prevent buckling. This would make the construction of the segments geometrically complex and larger. Another way to assure constant tension is to connect all sliders axially throughout the shaft as shown in Figure 6-B. By applying tension at the proximal segment all cables will conform to the shortest curve length throughout the shaft. This is a relatively simple way of preventing buckling without having to implement a lot more springs with a finely tuned stiffness to prevent buckling without influencing the joint angle. The downside of this setup is that the sliders need more axial space to displace for the bending of the segments in series. If two segments in series bend in the same direction on the same plane the sliders will have to move twice the distance. This means that the rigid segments have to be axially longer and the device will lose continuity. To solve this issue, the sliders and the cable will fuse functions by using timing belts as

steering cables as shown in Figure 6-E. By doing so, the segment's axial length is independent of the bending angle and only dependent on the timing belt pitch. To make sure the timing belts are facing the stoppers, they will be lead through channels in the segments. These channels will have an opening facing the stoppers who can radially displace to interlock with the timing belt.

The outer-shaft will have the same working principle as the inner-shaft shown in Figure 6-D. The cycle to achieve FTL motion is then established by alternating the propagation and locked state of each shaft as described in Figure 7. In the steering phase, the locked outer-shaft constrains the orientation of the relative proximal inner-segments so that only the distal segment will change its orientation as the timing belt is being pulled. The air tubes of the inner-shafts are then inflated to interlock the timing belts in their curve length and thus conserving the orientation of all inner-segments. The outer-shaft then releases the timing belts by deflating the three air tubes thus allowing the outer-shaft to conform to the shape of the inner-shaft when axially propagating. After this catch-up phase, the outer-shaft locks and the inner-shaft unlocks. The distal segment of the inner-shaft can now propagate as the relative proximal segments conform to the shape of the locked outer-shaft. This cycle can continue until an anatomical target is reached.

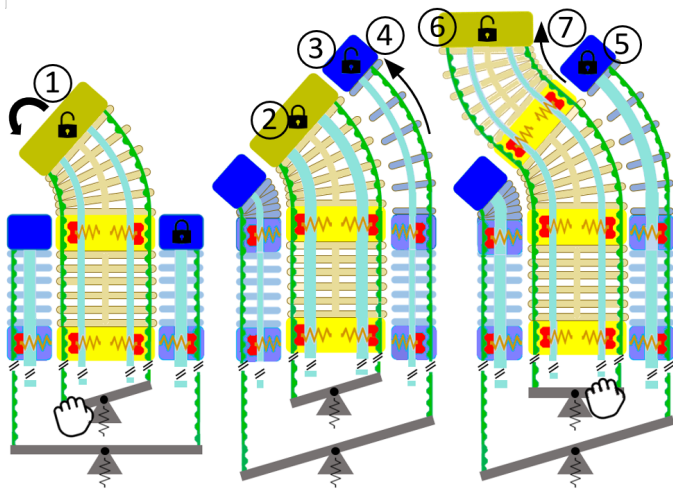


Fig. 7: A schematic side-section drawing of the concept medical device performing an FTL motion in seven steps. (1) The distal inner-segment is steered. (2) The inner-shaft is locked. (3) The outer-shaft is unlocked. (4) The outer-shaft is propagated. (5) The outer-shaft is locked. (6) The inner-shaft is unlocked. (7) The inner-shaft advances.

III. 3D DESIGN

The device consists of two concentrically aligned shafts that are mounted on their respective **stands** as shown in Figure 8-A. The inner-shafts and its stand can axially slide with respect to the outer-shaft and its stand and vice versa. Both shafts consist of segments that contain a rigid part called the **disk** and a compliant

part called the **joint**. The shafts have a set of three **air tubes** and three **timing belts** equally spaced from the center that run through designated channels in the shaft segments and are fixed to the tip of their shaft referred to as the **end-effector disk**. The timing belts are positioned furthest away from the centerline of the shaft to increase both the steering and the locking moment arm. Moreover, the bending resolution of the segment increases proportionally to this moment arm which is discussed in Section III-A2. To establish similar kinetic and kinematic values for both shafts, these channels have to be located at the same radius for the inner-shaft and the outer-shaft. Therefore they need to be geometrically integrated within their cross-sectional area as shown in Figure 8-B+C. In between the shafts, there are six strings of **guiding wires**, equally spaced and co-radial from the center, to ensure smooth translation. These wires are fixed to the end-effector disk of the inner shaft and fit in the slots of the outer-shaft while making tangent contact with the inner-shaft which secures their concentric alignment. The timing belts assume the curve shape of the segments and likewise, the segments adjust their orientation when the timing belts are pulled. The segment disks contain locking mechanisms that are actuated by the inflation of the air tubes. When the tube has inflated the **stoppers** inside the segment disks interlock with the timing belt and thus constrain the timing belt curve length between each set of segment disks. This will hold the configuration of the entire shaft. If the tubes are collapsed **elastic bands** push back the stoppers thus allowing the timing belt to translate through the segments and the shaft to change orientation. By alternating the state of the inner- and outer-shaft from locked to flexible during the propagation, the shaft can conserve the shape of the path taken by the end-effector as shown in Figure 7.

A. Inner-shaft design

The cross-section of the inner-shaft is shaped like a truncated triangle with concave sides and consists of four segments and an end-effector. Each segment consists of a disk and a compliant joint.

1) *Segment disk design:* The segment disk has several functions. First, it has to chamber the locking mechanism as shown in Figure 9. The mechanism consists of an elastic band wrapped around the air tube channel and a locking geometry called the stopper. The stopper contains two teeth that geometrically align with the teeth of the timing belt. The stoppers and elastic bands have to be chambered in a way that radial translation is the only DOF that is actuated by inflating and deflating the air tube. Secondly, the segment disk has to provide an axial passage for the air tubes and timing belts. An additional axial thickness equal to the pitch of the timing belt is added to assure smooth movement through the passage channels. The teeth of the timing belt have to face the stoppers at all times. Finally, the segment disk needs an

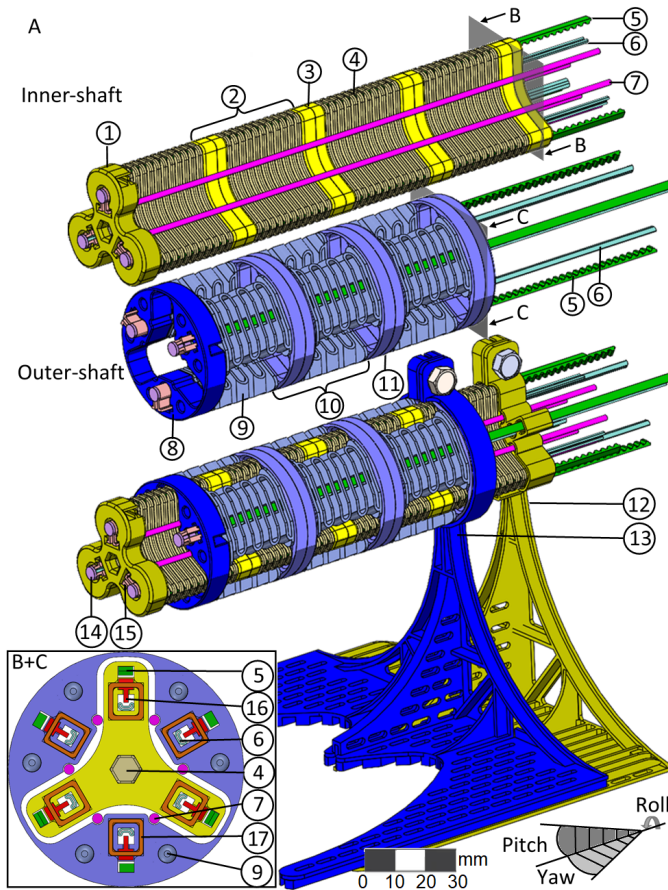


Fig. 8: CAD of the proof of concept FTL medical device with pneumatically actuated shape locks. The inner- and outer-shaft consists of segments (2 and 10) that have a rigid disk (3 and 11) and a compliant joint (4 and 9). The disks house stoppers (16) wrapped around with an elastic band (17). A set of three timing belts (5) and air tubes (6) are attached to the end-effector disk (1 and 8) and run through channels within the segments. The air tubes are closed off with plugs (14) that are secured with clamps (15). The shafts are mounted on their stands (12 and 13) and can fit and slide concentrically to each other. Six guiding wires (7) are placed between the outer perimeter of the inner-shaft and the inner perimeter of the outer-shaft to ensure smooth relative motion.

attachment geometry for the segment joint. The teeth of the stopper have an extra height equal to the thickness of the elastic band to wrap the elastic band around the stopper without interrupting the locking geometry. The elastic band has a chamber that goes around the air tube. The stopper is limited in its radial movement towards the air tube by a limit. For the air tube to interact with the stopper, an extra geometry is added at the back of the stopper that goes through the stopper limit. This extra thickness is the distance the stopper will travel when the tube is inflated. To get the best interaction with a collapsed and inflated tube, this thickness is fine-tuned. Since the stopper and elastic band are parts that are enclosed within the segment disk, the segment disk has to consist of a male and a female part. Both parts connect

with the hexagon pin to constrain the rolling angle. The hexagon pin is hollow to attach the segment joints with a similar concentrically aligned hexagon pin.

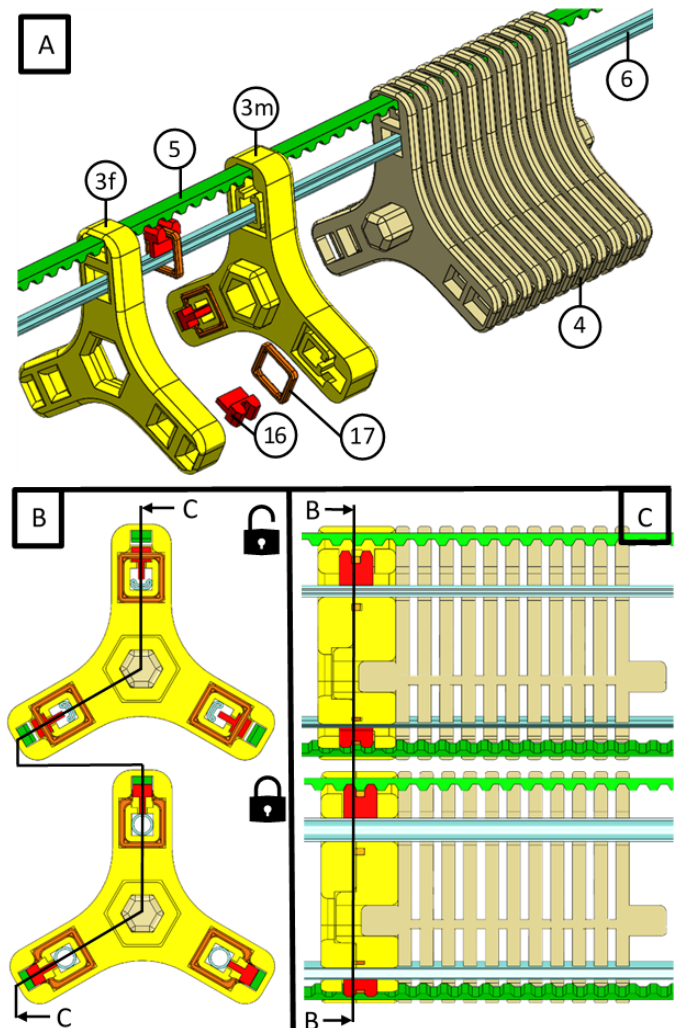


Fig. 9: Inner-segment parts and structure. (A) An exploded view of the inner-segment. Three equally spaced chambers inside the male (3m) and female (3f) segment disk (3) house the locking mechanism which consists of an elastic band (17) wrapped around the stopper (16). Radially co-linear to these locking mechanisms are passages for the air tube (6) and timing belt (5). These passages are also present in the segment joint (4). Only one set of a timing belt and an air tube is drawn to show their alignment. (B) A cross-section view of an unlocked (top) and a locked (bottom) configuration within the segment disk. When the air tube inflates the stoppers are pushed radially outward and interlock with the timing belt. The elastic band pushes the stoppers back when the air tube is collapsed. (C) A side-section view of the segment in an unlocked and a locked state.

2) *Segment joint design:* The function of the segment joints is to connect the segment disks such that they have a free pitch and yaw angle with respect to each other. Furthermore, they have to provide a passage to the air tubes and timing belts. Since the timing belts are rectangular, they are a lot more compliant to bending around the axis parallel to the teeth width. Therefore, the

timing belts will twist when they are bend perpendicular to their width. To account for this twist the passage slots for the timing belts are wider. The inner-segment joint has a flexible backbone that has thin disks attached to guide the tubes and timing belts along the curvature. The backbone prevents the joint from being compressible which is crucial to obtain proper bending angles when tension is applied to the timing belts. The joints contain a hexagonal connection pin at its axial ends to attach to the segment disks.

Kinematic analysis

The height of the joint depends on the change of curvature length imposed by the bending force. The amount of space between the thin disks is fixed and their displacement is determined by the kinematic analysis shown in figure 10. The relation between the bending angle and the timing belt translation had to be found. According to this relation, the joint was designed for the right bending angle. The length of the timing belt between the two segments $L(x)$ depends on the distance x traveled by the timing belt. As the timing belt translates, the joint with height h_j will bend and assume a curve shape with a length h_j , a bending angle with its vertical θ , and a radius of curvature r_j . The model assumes a constant curvature across the height of the joint. Initially the cable length $L(x)$ is equal to the joint height h_j . The traveled distance of the timing belt x can be expressed as follows:

$$x = h_j - L(x) \quad (1)$$

Since the traveled distance of the timing belt is equal to the length of timing belt that is pulled. The radius of curvature r_j can be expressed as $\frac{h_j}{\theta}$ and the curve length of $L(x)$ can be expressed as $(r_j - r_s)\theta$, where r_s is the radius of the segment disk. Substituting these two equations to get rid of the unknown r_j gives:

$$L(x) = h_j - r_s\theta \quad (2)$$

Substituting this in Equation 1 will cancel out the joint height h_j and gives the relation between the timing belt travel distance x and bending angle θ :

$$x = \theta r_s \quad (3)$$

A larger bending angle will add dexterity to the device but makes the concentric sliding movement more difficult since the shaft contains sharper turns and the rigid segment disks are not infinitely thin. From the design requirements, an angle of 30 degrees is applied. Therefore, according to Equation 3, the timing belt will translate approximately 8.5 mm. This means that the space within the thin joint disks has to add up to at least 8.5 mm to be able to perform a 30-degree angle. Ultimately each segment has a bending resolution of 30 degrees / 8.5 mm \approx 3.5 degrees per mm. Since the interlocking teeth have a pitch of 2.5 mm, each segment has a resolution of 2.5 mm \times 3.5 degrees per mm \approx 8.8 degrees.

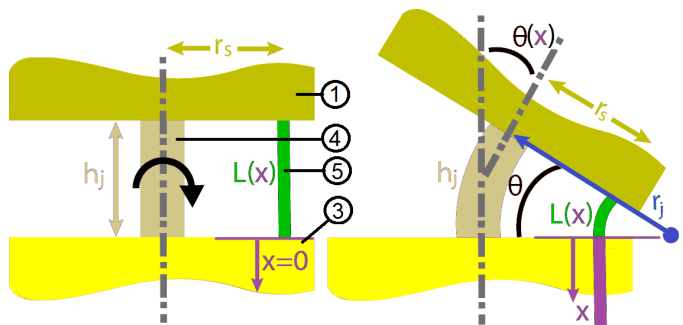


Fig. 10: **Schematic representation of the bending geometry.** The timing belts (5) pass through the segments (3) at a distance r_s from the center. The segments are connected with a flexible joint (4) with height h_j . When the cable is pulled a distance x it will bend the joint with bending radius r_j and an angle θ between the centerline of the distal segment (1) and the centerline of the proximal segment. The cable then assumes a curve length $L(x)$.

3) *End-effector disk and stand design:* The function of the end-effector disk is to fix the air tubes and timing belts. Since the inner-shaft is the leader, the six strings of guiding wire have to be attached to its end-effector disk to ensure smooth movement at the catch-up phase. Figure 11 shows how each of these parts are fixed to the end-disk. A clamp around the plugged tubes secures the tube end in the designated slots. This arrangement will allow for maintenance if the tube is not airtight and secures the tube in position without putting much stress on the silicone. The timing belts slide in tangentially to a set of teeth. The hexagonal hole connects to the distal segment joint.

The stand is an L-shaped corner with a clamp that wraps around the proximal segment disk and contains passages for the guidewires, air tubes and, timing belts from the outer-shaft. The clamp can be tightened around the proximal segment disk with a screw as shown in Figure 8. The stand contains ridges to increase stiffness and linearly guide the axial translation with respect to outer-shaft stand.

B. Outer-shaft design

The outer-shaft is circular and consists of three segments and an end-effector. Each outer-segment consists of a rigid disk and a compliant joint.

1) *Segment disk design:* In addition to housing the locking mechanisms, providing passage to the timing belts and air tubes, and allowing connection to the segment joints, the outer shaft also has to constrain the location of each string of guiding wire. Six indentations alongside the inner perimeter of the outer-shaft disk make sure the guiding wires stay in place. The male and female parts of the segment disk are connected by six pins as shown in Figure 12. The pins are hollow to allow for the attachment of the segment joint similar to the inner segments. Since the connection pins are off-center

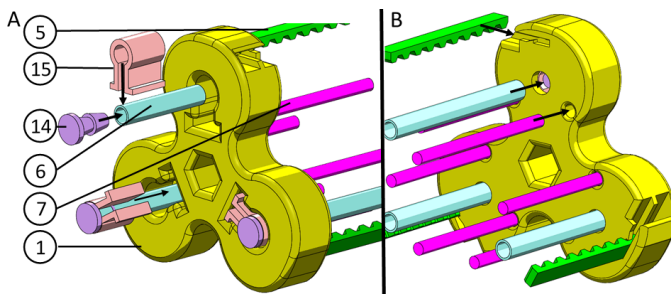


Fig. 11: **Exploded views of the inner-shaft end-effector disk.** (A) An exploded front view of the inner-shaft end-effector disk (1). The air tubes (6) are closed off with plugs (14) that are secured with clamps (15) which squeeze in the slots. (B) An exploded back view of the inner-shaft end-effector disk. The six guidewires (7) are fixed inside the holes. The timing belts (5) tangentially slide in the slots that geometrically constrain their axial movement.

they do not have to be hexagonal shaped to constrain the rolling angle.

2) *Segment joint design:* The outer-shaft joint consists of three separate identical compliant springs equally spaced around the center. Since the outer shaft can not have a backbone because of the concentric alignment, it is aimed to contract and extend the curve length variation at the inner and outer edges respectively. The compliant springs have to be able to contract and extend the distance of 8.5 mm resulting from Equation 3 to be able to conform to the shape of the inner shaft. Similar to the segment disk the compliant springs contain indentations to hold the guidewire in place.

3) *End-effector disk and stand design:* The only difference in function with the inner-shaft end-effector disk is that the outer-shaft end-effector disk, shown in Figure 13, does not fix the guidewires but instead has to contain the six indentations to hold the wires in place.

The stand contains ridges on the opposite side to increase stiffness and linearly guide the axial translation with respect to the inner-shaft stand. A clamp is fixed to the stand that wraps around the proximal segment and tightens with a screw, Figure 8.

IV. PROTOTYPING AND ASSEMBLY

Apart from the air tubes, the timing belts, and the elastic bands the parts for the proof of concept prototype were 3D-printed using the Creality Ender 3 with a 0.4 mm diameter nozzle. Furthermore, the guiding wires to establish a smooth relative translation between the alternating shafts, are strings of filament placed between the shafts. Since the set of six guiding filament strings can be seen as six bending springs in parallel; their stiffness is proportional to their number. To prevent a dominating stiffness from these wires, TPU filament with a 1.75 mm diameter was chosen as its stiffness is negligible relatively to the stiffness of the segment joints. For the prototype design, it means that the dimensions partially depended on commercially available parts. The

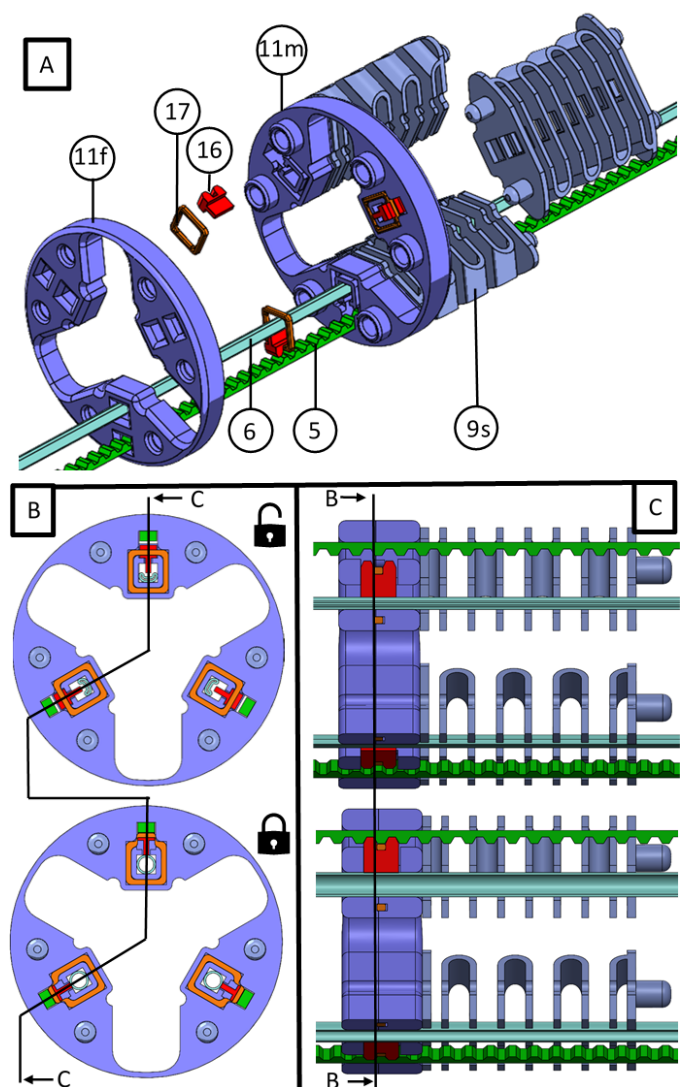


Fig. 12: **Outer-segment parts and structure.** (A) An exploded view of the Outer-segment. Three equally spaced chambers inside the male (11m) and female (11f) segment disk (11) house the locking mechanism which consists of an elastic band (17) wrapped around the stopper (16). Radially co-linear to these locking mechanisms are passages for the air tube (6) and timing belt (5). These passages are also present in the segment joint (9) which consists of three compliant springs (9s). Only one set of an air tube and a timing belt is drawn to show their alignment. (B) A cross-section view of an unlocked (top) and a locked (bottom) configuration within the segment disk. When the air tube inflates the stoppers are pushed radially outward and interlock with the timing belt. The elastic band pushes the stoppers back when the air tube is collapsed. Six equally spaced half-circular indentations form slots to secure the guiding wires. (C) A side-section view of the segment in an unlocked and a locked state.

timing belts were axially reinforced with glass fiber and had a width of 5 mm and a 2.5 mm pitch. This timing belt was cut in half to reduce the width and therefore the diameter of the device. To make this possible the device shown in Figure 14 was designed to steadily hold a knife in the middle of a geometry that guided the timing belt

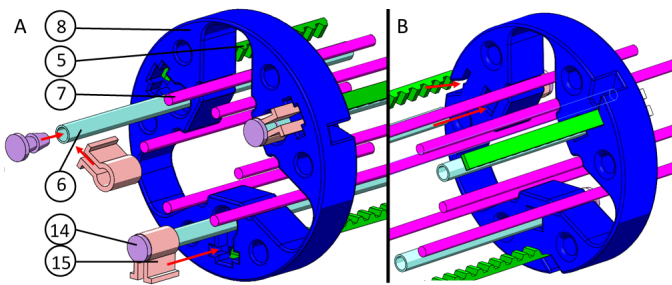


Fig. 13: **Exploded views of the Outer-shaft end-effector disk.** (A) An exploded front view of the Outer-shaft end-effector disk (8). The air tubes (6) are closed off with plugs (14) that are secured with clamps (15) which squeeze in the slots. (B) An exploded back view of the Outer-shaft end-effector disk. The six guidewires (7) fit concentrically to the slots located along the inner perimeter. The timing belts (5) tangentially slide in the slots that geometrically constrain their axial movement

through it. The thickness of the timing belt was 1.5 mm of which half was the tooth height. The elastic bands are orthodontic elastic bands with a diameter of 4.8 mm, a thickness of 0.5 mm, and a height of 1.2 mm. The silicone tubes were 2.6 mm in diameter with a wall thickness of 0.3 mm.

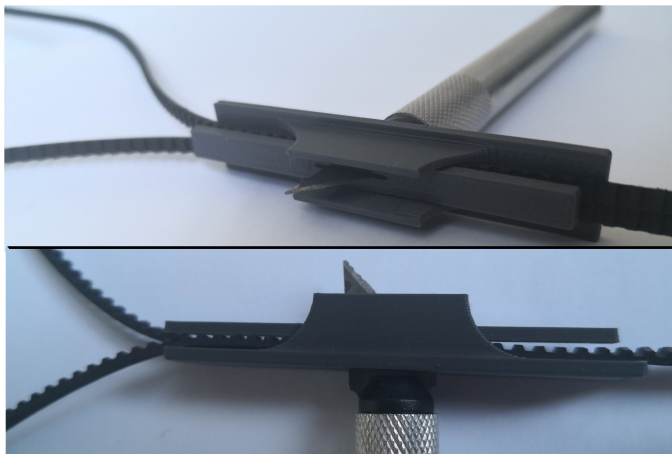


Fig. 14: **A picture of the timing belt cutter.** A guide leads the timing belt through a knife located at the center splitting the belt in half.

All parts of the device are designed to allow printing without supports that would greatly interfere with the geometry. The inner-shaft has a tangent connection with the three rectangular locking mechanisms to allow for printing radially without supports. This will make the printing of the inner-segment joints faster, more reliable and, most importantly, it conserves its functional integrity. To allow for such a cross-sectional shape, the slots for the guiding TPU filament strings were exclusively located in the outer-shaft as shown in Figure 8. The inner-shaft only makes tangent contact to these guidance strings. Since the outer-shaft joint consists of three separate compression springs these

indentations for the guidance strings did not pose a problem for printing without supports. The nozzle size limits the recommended wall thickness to ≥ 0.8 mm for geometries printed perpendicular to the print bed. A detailed overview of the print settings and the dimensions of each part is shown in Appendix A. Pictures of the parts before and after assembly are shown in Appendix B.

To assemble the inner shaft the air tubes were closed off by filling the ends with silicone glue and plugging them with a 3D-printed barbed plug. These plugs were surrounded by 3D-printed clamps. The tubes were then put through the designated holes in the end-effector disk until the clamps were housed in their designated slots. Then, the timing belts were attached to the end-effector disk by sliding them in the designated slots. The last attachment to the end-effector disk were the six strings of TPU filament glued in their designated holes. The set of three tubes and timing belts can then be put first through the channels of a segment joint and then a segment disk. When pushing the set of air tubes through the segments the stoppers were pushed radially outward with tweezers. Finally, the set of timing belts were pushed through their designated passages. This is repeated for every segment until the proximal segment disk is attached. To assemble a segment disk an elastic band was wrapped around each stopper. These three stoppers and elastic bands were then placed in their designated slots of the male segment disk. The elastic bands were stretched over the edge of the air tube passage and then closed off by the female segment disk. The outer-shaft was assembled identically with the exception that three compliant springs were attached to each segment disk and that the end-effector does not fix any guidance strings. The inner-shaft was then slid inside the outer-shaft with the TPU strings concentric to the rounded slots of the outer-shaft segments. Finally, the two shafts were clamped onto their stands, and the air tubes were attached to 3D-printed pneumatic barbed fits. To hold the syringe plungers at a certain position a slider-crank mechanism shown in Figure 15 was made. A joint in this mechanism can be tightened and constrain the plunger translation with friction forces.

V. TESTING AND RESULTS

The complete shaft of the prototype weighs 90 g where one inner-shaft segment weighs 11 g and one outer-shaft segment weighs 13 g. The device has 9 DOFs and a total bending angle of 90 degrees for a radius of curvature of 85 mm.

A. Operating force test

As the shaft of the device is in a stiff state where the stoppers interlock with the timing belt, the segments should hold their orientation. However, when external forces react onto the shaft the interlocking geometry might slip. The force at which this slipping occurs and thus the configuration of the shaft is lost, is called

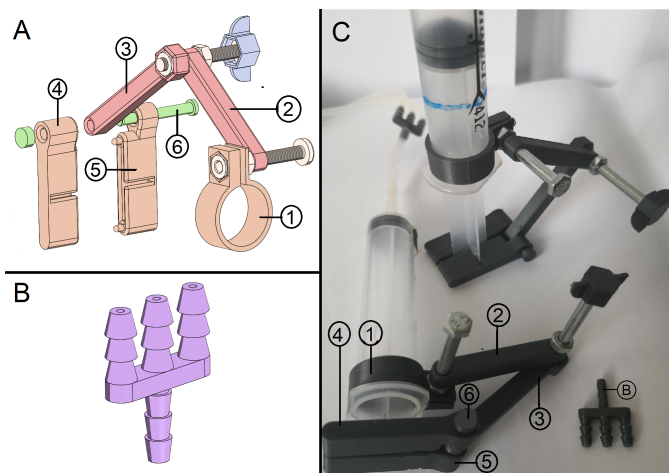


Fig. 15: **CAD drawing and picture of pneumatic attachments.** (A) A CAD drawing of a syringe clamp. The circular clamp (1) is tightened around the syringe chamber with an M4 bolt. This bolt is used as a hinge by a link (2). Another link (3) hosts a nut that allows for the two links to be compressed against each other by tightening the connection. The proximal disk of the syringe piston is locked in between a female (4) and male (5) geometry lock. A pin (6) attached the link to this lock allowing one DOF. (B) A pneumatic fitting with one input and three outputs. (C) A picture of the pneumatic attachment (A) and (B) assembled.

the operating force. Since an important aspect of FTL motion is to operate without relying on anatomical reaction forces, it might seem unnecessary to calculate how much force the shaft can hold before slipping. Nevertheless, external forces will occur as the alternating shafts advance and catch up. Furthermore, if the shafts contain working lumen that host instruments (i.e. needle, grasper) external forces will be exerted onto the shaft when interacting with the anatomy (i.e. biopsy). The test setup to measure the operating force is shown in Figure 16. For different orientations, the end-effector is attached to a scale as the air tubes are expanded. The proximal segment is then held and pulled down parallel to the cable. The scale holds the highest value until the teeth of the timing belt slip away from the stopper. This measurement is done three times for three different configurations. The results are shown in Table I.

The operating force decreases as the distal segment is further away from the proximal segment because the moment arm increases.

B. Precision test

1) *Tip bending test:* In order to steer the tip the outer-shaft has to conserve the configuration of the inner-shaft and constrain the bending of all but the distal inner-segment. To see how much the shaft displaces an overlap figure was made as the distal inner-segment was bent with a locked outer-shaft. To visualize the effect of the locks, the same steering actuation was performed for an



Fig. 16: **Picture of the operating force test setup.** The prototype (1) is attached to the scale (2) with a cable (3). As the shaft assumes several configurations the air tubes (4) are expanded with a syringe (5). The shaft is then pulled down until a timing belt (6) tooth starts slipping across the stopper.

TABLE I: **Operating force of the inner- and outer-shaft for various configurations measured three times.**

Inner-shaft				Outer-shaft			
Configuration:	Tension [N] till tooth slip:			Configuration:	Tension [N] till tooth slip:		
	1	2	3		1	2	3
	10.29	8.47	8.91		8.48	11.97	9.56
	1.30	2.21	2.27		1.29	1.75	1.87
	6.02	2.83	3.88		5.37	2.17	2.67

unlocked outer-shaft, Figure 17. The constraining effect of the locked outer-shaft is clearly visible.

2) *FTL advancement test:* To demonstrate the ability to advance in an FTL manner, the shaft attempted to follow a C- and S-curve. The motion was performed in two ways. First, the steering and advancing forces were only supplied by pulling the timing belts and translating the stands respectively. Second, the steering was assisted by bending the segments and pulling the timing belt. The advancing motion was assisted by not only pushing

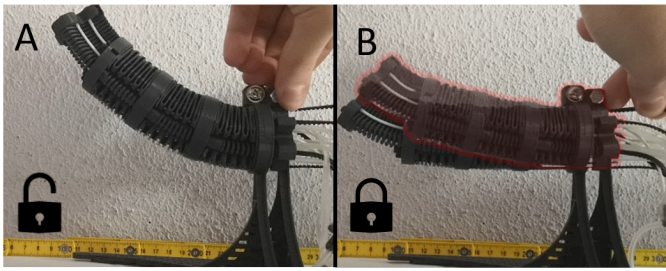


Fig. 17: **Picture of the distal segment actuation.** (A) The distal segment is actuated with both the inner- and outer-shaft unlocked. (B) The distal segment is actuated with the outer-shaft locked. The red hue indicates the intermediate displacement of the shaft.

the stand put also pulling the distal segment, Figure 18. This is done to reduce the forces acting on the proximal segments. The path is best followed at the first cycle and loses the desired configuration towards the end of the advancement. When assisted with hands on the shaft the shape is conserved more successfully.

3) *FTL retraction test*: To test whether the shaft cannot only advance towards a target but also retract from it, an arbitrary S-curve is set as starting configuration. The shaft is then retracted in an FTL manner, Figure 19. Similar to the advancement the path is conserved during the early stages of the motion but is lost towards the end of the retraction.

VI. DISCUSSION

A. Evaluation and improvements

From the performance test, it can be seen that the shaft often diverts from the path after the third step. Especially for tests without assistance, the proximal segments seem to slack under the weight of the shaft. This result does correlate with the operating force test where it was clear that the teeth of the locking geometry started slipping for lower forces at the proximal segments. The slip of the timing belt teeth from the stopper occurs because of the locking geometry. Since the teeth of the timing belt do not have a surface perpendicular to the axial direction, the shape lock has a radial force component as shown in Figure 20-A. As a result of the tension in the timing belt this radial force component translates the stopper away from timing belt. This means that the strength of the lock is dependent on the radial force imposed by the inflating air tube. Ideally, the teeth would have a wedging tip to enter the interlocking geometry and then settle their parallel teeth surfaces perpendicular to the axial direction of the shaft. The distance that needs to be translated by the stoppers depends on the length of this surface. The air tubes should be optimized to initiate this distance to avoid the use of larger tubes than necessary. The increase in radial expansion of the air tube is equal to the diameter minus twice the wall thickness. To translate the 0.75 mm teeth height the air tube could have been a lot smaller than 2.6 mm. however, the collapse and inflation of the

air tube is dependent on the ratio of the diameter and wall thickness and can therefore not be too small as the wall thickness is quite a limiting factor in the production of narrow tubes.

It was also observed that the elastic bands had a force that would push the stoppers into the air tubes when expanded. This was countered by increasing the length of the stopper to compensate for the lack of translation. Furthermore, the stoppers would sometimes slide towards the sides of the tubes when inflated and thus translate even less. This could be countered by increasing the width of the stopper but then a collapsed tube could not wrap around it and corrupt the flexible state of the shaft. Random failures of radial stopper translation might be the reason for inconsistent operating forces seen in Table I.

Since the timing belts twist when bend perpendicular to their teeth, the dimension of the channels in the segment joints was increased. Undesirably, this allowed for the timing belts to buckle when external forces were applied to the shaft. This caused undesired changes in shaft configuration as the length of the timing belt was not restricted to the shortest curve length. This is also the cause for undesired shaft movement during the steering phase as demonstrated in Figure 17. To prevent ensure that the shortest curve length is locked a more symmetrical bending timing belt is needed. A commercial alternative was proposed in Section VI-B2 - Design alternatives - Locking mechanisms.

The advancing motion was met with some friction which leads to a difficult catch-up movement of the outer-shaft. The surface of TPU filament is less smooth than i.e. nylon or PLA. Therefore, the relative motion of the shafts was met with a slight stick-slip friction. The surface of the filament could be treated or the guidewires could be replaced by a different material with a similar stiffness. Since the filament is rolled onto a spool the strings of stiffer filament have a plastic curve that greatly influences the bending stiffness in one plane. To get rid of this curve the filament strings would have needed some treatment to bend straight.

B. Design alternatives

1) *Tube arrangement*: A great convenience that comes with pneumatic actuation in the form of an expanding air tube, is that the force and displacement are equal in all radial directions. This would allow for actuating multiple locking mechanisms with a single tube as shown in Figure 21-A. However, this is only possible for the inner shaft since it has a geometry at the centerline. To have the same steering and locking moment the mechanisms have to be corradial to the outer-tube. This would mean that the stoppers for the inner-shaft have to be a lot longer as shown in Figure 21-B. To reset the lock a single elastic band could wrap around all three stoppers. Moreover, the tube has to run through the whole system meaning that a compliant joint with a

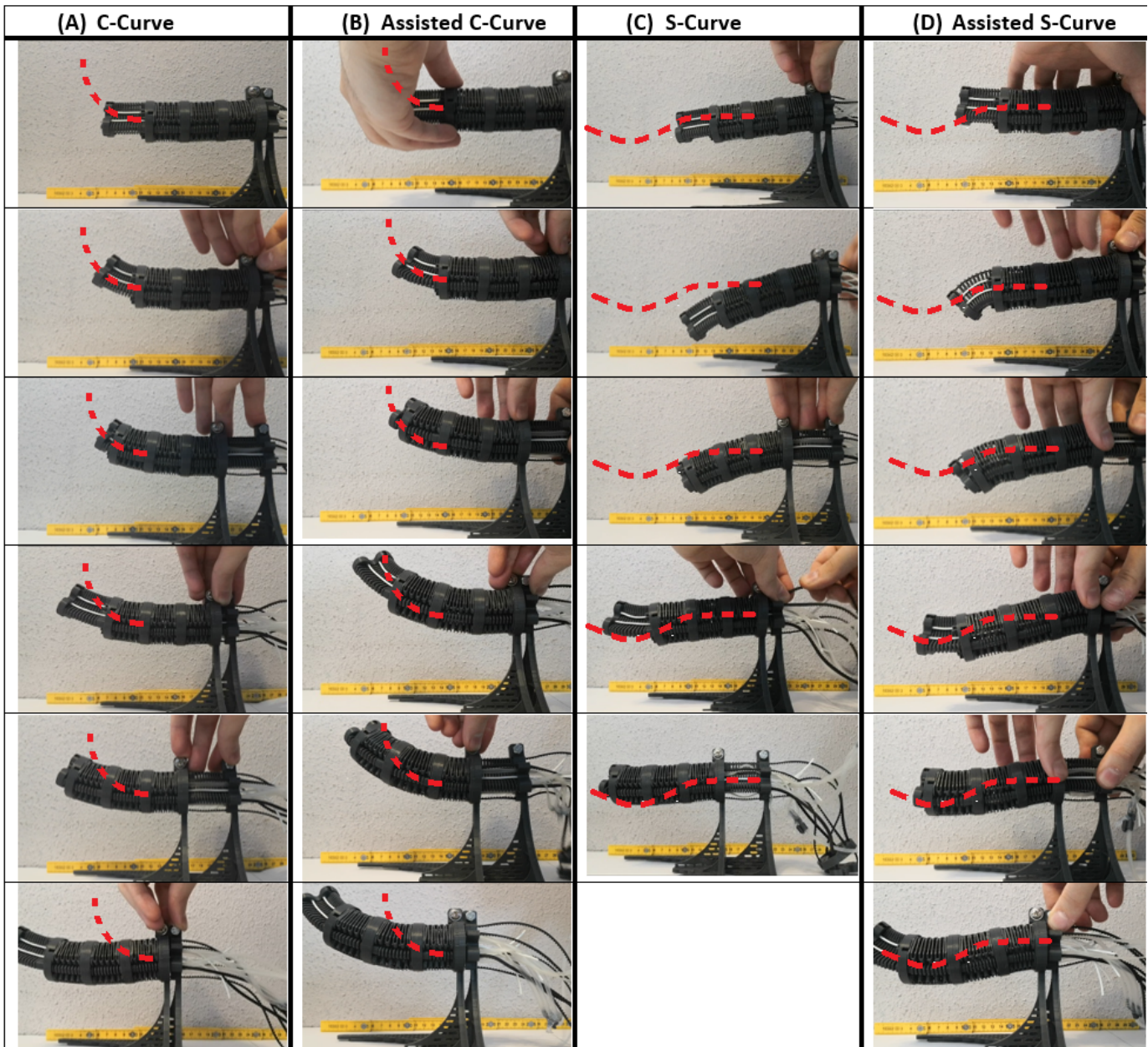


Fig. 18: **Picture of the prototype performing FTL movement.** (A) The device attempting to advance in an FTL manner with a C-curve path. (B) The segment bending and advancing motion are assisted with hands on the shaft. (C) The device attempting to advance in an FTL manner with an S-curve path. (D) The segment bending and advancing motion are assisted with hands on the shaft.

backbone is not possible. This could be solved by using hollow ball-and-socket joints instead as shown in Figure 21-C. Another design that reduces the number of tubes by actuating multiple mechanisms is shown in Figure 22. By reversing the locking direction for one shaft from radially outward to radially inward, the mechanisms can lock and unlock simultaneously for pneumatic actuation. The springs reset the stoppers accordingly. This design means that the shafts are both briefly unlocked and therefore the lock alternation has to actuate rapidly.

2) *Locking mechanism:* If the device can be miniaturized to the point where the stopper is not

affected by gravity, the spring (elastic band) would not be necessary. Because the elastic band needs a chamber around the air tube channel, the stopper originally had a geometry to reach the air tube as shown in Figure 23-A. Without the elastic band or any other spring, the stopper chamber can be smaller as shown in Figure 23-B. An even smaller diameter could be achieved if the edge of the segment disk would serve as a stopper as shown in Figure 23-C. Instead of pushing a locking structure in the timing belt, the inflated tube will push the timing belt into the edge of the segment disk. Although this arrangement will allow for a small channel going

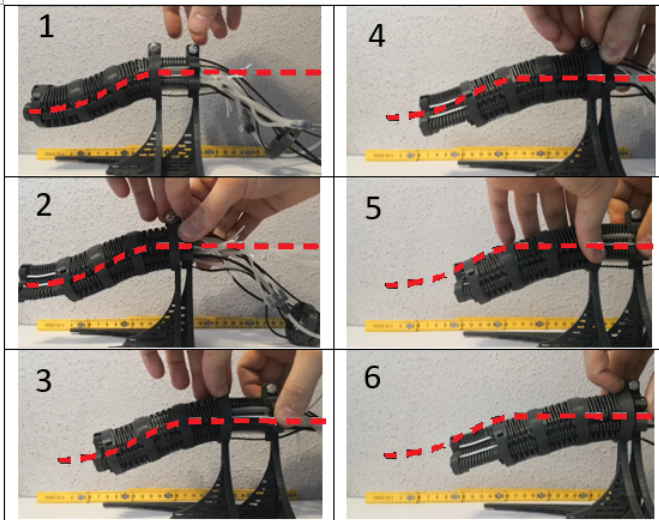


Fig. 19: Picture of the prototype performing an FTL retraction in 6 steps.

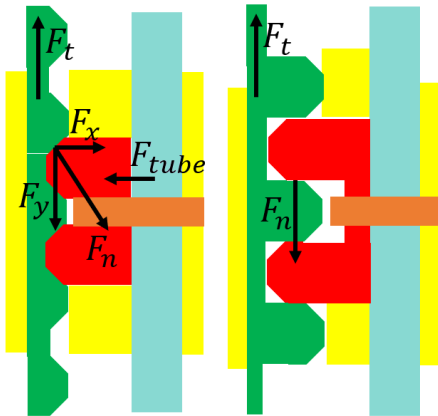


Fig. 20: A side-section view of a shape locking mechanism. On the left, the locking geometry contains teeth with angles that induce a normal force F_n perpendicular to the tooth surface. This normal force holds the tension F_t in the timing belt with its vertical component F_y but also introduces a horizontal component F_x . This horizontal components works in the opposite direction of the tube expansion force F_{tube} . On the right, the teeth have a surface perpendicular to the timing belt tension. Now the normal force is equal and opposite to the timing belt tension.

through the shafts without any chambers, it assumes the timing belt does not twist and remains stretched close to the air tube. In reality, the timing belt requires more guidance for reliable locking. To prevent twisting when bending a commercially available round cable with an interlocking geometry could be used as shown in Figure 23-D [51]. However, since the locking geometry is at an angle the force component problem depicted in Figure 20 can not be solved by design. Originally these cables can be wrapped around pulleys and provide a driving force similar to timing belts. As opposed to timing belts

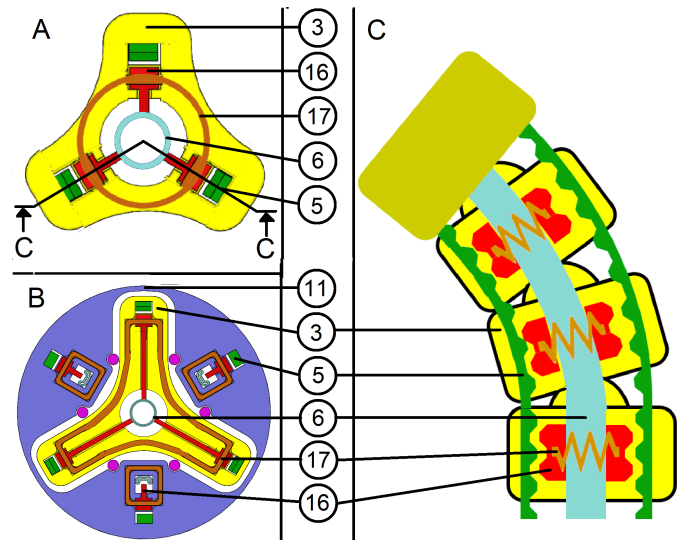


Fig. 21: Alternative air tube arrangement operating three stoppers. (A) A schematic cross-section view of an alternative inner-shaft segment-disk (3) with the air tube (6) located in the center actuating three stoppers (16) at the same time. A single elastic band (17) can now be wrapped around all three stoppers. (B) A schematic cross-section view of an alternative inner- and outer-shaft segment-disks (11). To have the mechanisms corradial the stoppers have to be longer. (C) A side-section view of the alternative inner-shaft with hollow ball-and-socket joints instead of compliant joints.

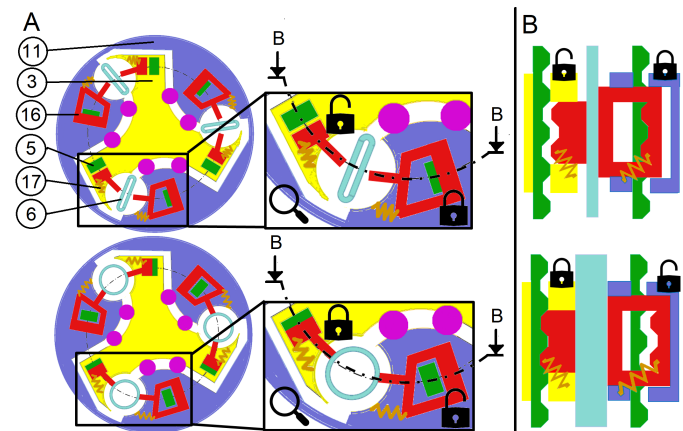


Fig. 22: Alternative air tube arrangement operating two shafts. (A) A schematic cross-section view of an alternative inner- and outer-shaft segment-disk. Three air tubes actuate two stoppers each simultaneously. As the air tube (6) inflates the stopper (16) for the inner-shaft (3) is pushed towards the timing belts (5) and the stopper for the outer-shaft (11) is pushed away from the timing belt. The springs (17) reset the stopper position when the air tube is collapsed. (B) A side-section view of the mechanism in Figure (D). The stoppers and timing belts face the same direction while the air tube pushes the stoppers radially in the opposite direction.

though, these cables are designed to operate in multiple planes.

If gravity cannot be ignored and a mechanism is needed to reset the stopper position, magnets could

replace the elastic bands as shown in Figure 23-E. As the tube is collapsed the magnets fixed in the segment disks will pull the stoppers away from the timing belts. Conversely, the inflation of the tubes has to overcome this magnetic force when locking the shaft. This mechanism could turn the device EM incompatible. Another solution is compliant springs within the segment disk as shown in Figure 23-F. But, this would only function with a very thin or long structure like a flexible beam. Therefore, the height of the segment disks would increase. As opposed to elastic bands which require an increase in diameter, the compliant springs would require an increase in height. This is generally preferred over an increase in diameter since the height is a dimension in the direction of the advancement whereas the diameter is a dimension in the direction of the anatomy. A printer capable of printing two different materials could print a smaller flexible geometry functioning as a spring instead. As opposed to radial translation the stoppers could also rotate around a joint within the segment disk as shown in Figure 23-G. As the air tube inflates the stopper rotates into the timing belt. This would require an interlocking geometry that accounts for the change of orientation around the joint. Note that this is only a change in the kinematics and does still require a resetting force, in this case possibly a torsion spring.

Other than reducing the diameter, changing the locking mechanism could also change printing possibilities. The arrangements in Figures 23-B, -C, -D, and -F eliminate the need to insert non-3D-printed parts inside the segment disks. This means that the segment joints and disks can be printed as one part with the locking geometry inside, greatly reducing the assembly time. Note that the stoppers in these single print solutions would have to sustain their DOF after printing. Furthermore, if a fracture occurs the whole shaft would need replacement rather than one part. A visual demonstration of replacing a part is shown in Appendix C.

A more radical design alternative that uses pneumatically actuated shape locks, Figure 24. As mentioned in the Section II - Conceptualization, universal joints can have integrated shape locks since the axes rotate in one plane. A working principle of this angle locking mechanism is shown in Figure 24. An air tube going through the center of the joint crossing pushes pistons when inflated. These pistons serve as stoppers and displace radially to the air tube and interlock with the joint. Compression springs around these pistons reset the mechanism when the air tube is collapsed. Similar to the design shown in Figure 21-A this is only suitable for the inner-shaft. Another alternative design is to fuse the function of the spring and the guidewires.

In Section IV - Prototyping and assembly the choice of TPU filament is justified by not wanting to overwhelm the bending stiffness of the shaft imposed by the joints. Conversely, the stiffness could be determined by these

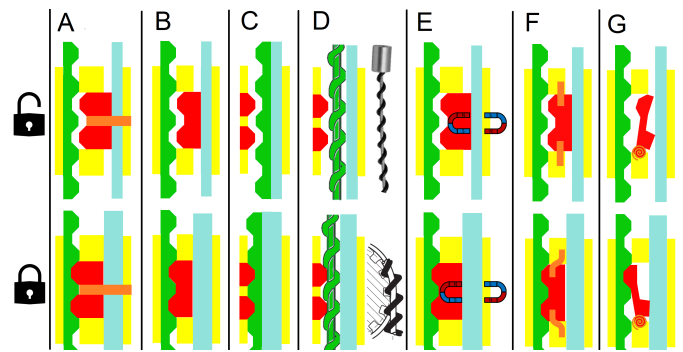


Fig. 23: Side-section views of various locking mechanisms located inside the rigid segment disk (yellow). The mechanisms consist of stoppers (red) that interlock with the timing belts (green) as the air tube (blue) is inflated. When the air tubes are collapsed the springs (orange) pull back the stoppers. (A) The original setup with an elastic band as spring. (B) A setup without spring where the stopper is assumed not affected by gravity. (C) A setup where the stopper is a merged part of the segment disk. The timing belt switched places with the stopper and displaces into the stopper. (D) A similar setup as (C) where the timing belt is replaced with synchronous drive cables [51]. A picture of the synchronous drive cables is shown next to the side-section view. A schematic drawing shows how the synchronous magnetic cable interlocks with a pulley. (E) A setup where magnetic force resets the stoppers as opposed to elastic tension. (F) A setup that uses compliant springs. (G) A setup that uses a torsion spring to reset the stopper that interlocks by rotating into the timing belt teeth.

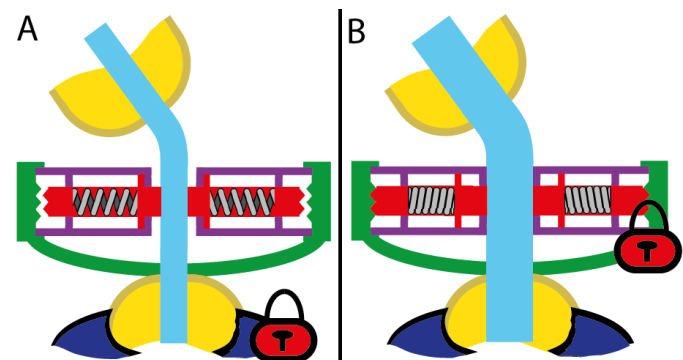


Fig. 24: A schematic drawing of a pneumatically actuated shape lock in a universal joint. (A) As the air tube (blue) is collapsed the joint (green) is free to rotate around the journal cross (purple) and change the orientation of the segment (yellow). (B) When the air tube inflates the stoppers (red) push their interlocking geometry into the joint and constrain the rotation. Joints inside the journal cross ensure the stoppers reset when the air tube is collapsed.

guiding wires whereas the joint would only constrain the distance between the segment-disks. By doing so an interlaced FTL medical device as presented by Kang et Al. shown in Figure 25 could be made [39]. To transform the friction lock to a shape lock the deployment rods can be replaced by something with an interlocking geometry such as the synchomesh shown in Figure 23-D. Furthermore, the piezo-actuator can be replaced by a

pneumatic one.

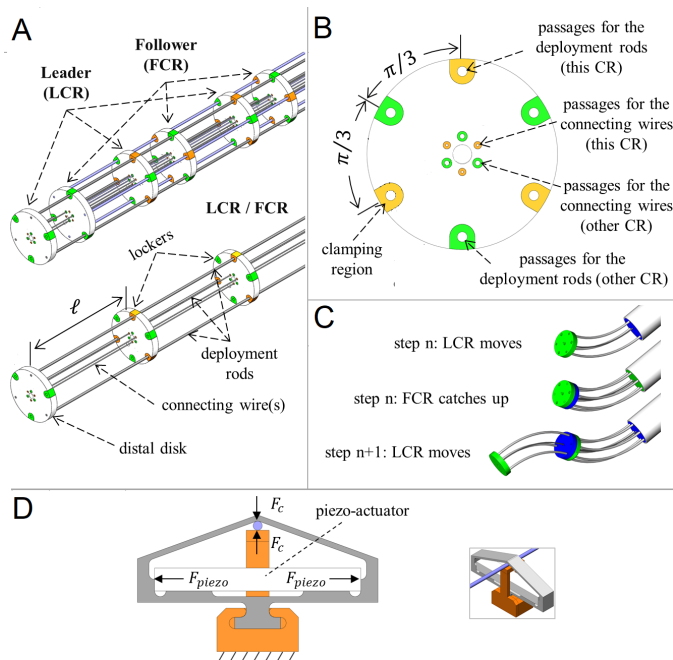


Fig. 25: **An interlaced medical FTL continuum robot (CR)**. Adapted from [39]. (A) Two identical continuum robot shafts are concentrically interlaced. Deployment rods supply concentric movement to the disks shown in (B). The connecting wires ensure an equal and consistent distance l between the disks. Both the rods and the wires are fixed to the distal disk. Lockers inside the disks clamp the deployment rods as shown in (D). The Leader Continuum Robot (LCR) and the Follower Continuum Robot (FCR) are $\frac{\pi}{3}$ rad apart. By alternating the clamping of the rods an FTL motion can be realized as shown in (C). (B) Front view of a disk. The passages are equally spaced around the center and contain clamps that lock the deployment rods in their orientation. (C) The CR performing an alternating FTL motion in steps. When the FCR is locked, the LCR advances. Afterward the LCR is locked and the FCR catches up. Finally, the FCR is locked and the cycle continues. (D) Friction-locking mechanism. The piezo-actuator clamps (F_c) the deployment rods by elongating the base of the lock with piezo-forces (F_{piezo}).

C. Future work

Producing a medical device with 3D-printed parts is suitable for prototyping but more conventional materials and production methods might be needed to have an optimal device. Furthermore, as a proof of concept, the device is limited to manual steering, locking and advancing. Ideally, the operator of the device only steers the end-effector and regulates the travel speed with a steering module. The alternating motion could be automated as an output of these input variables. The device has the potential to be fully robotic containing no more than seven actuators independent of the number of segments. One pump for each shaft can trigger the locking sequence and a linear motor for each shaft will actuate the advancing motion. Since the steering

mechanism contained no novelty it was not much elaborated in the 3D design. The use of timing belts does make it suitable for steering with pulleys fixed to step motors. These motors could precisely pull and release the timing belts depending on the desired angle of the distal segment. The outer-shaft needs a mechanism that keeps the timing belts in tension. During testing the air tubes and timing belts had been buckling between the outer-shaft and the inner-shaft stand as the advancing or retracting motion was initiated.

A more passive and manually operable device might however be desired in low- and middle-income countries due to constrained financing capacities [52], [53]. Many devices in developed countries do not work when arriving at counties in development [54]. The prototype of this work shows how relatively dexterous and highly articulated devices could potentially be produced. The complete shaft of the prototype has a material cost of 6 euros and 60 cents. One inner-shaft segment has a material cost of 27 cents to print. Adding the cost of the timing belt (23 cents) and air tube (52 cents) for one segment length, and three elastic bands (21 cents) gives a total of 96 cents. For one outer-shaft segment the total material cost is 92 cents. This means that adding 2 extra DOFs, 30 mm of length, and 30 degrees of reach to the shaft will cost only 1 euro and 88 cents of materials. The syringes are 30 cents each.

To improve the shape lock with teeth perpendicular to the axial direction of the shaft, as shown in Figure 20, an alternative to commercially available timing belts is needed. Finally, the proof of concept design had a lot of the cross-sectional area that can be used to host working lumen. After miniaturization, this area will decrease but the relative locations are still suitable.

VII. CONCLUSION

A novel alternating FTL device with pneumatically actuated shape locks was designed, produced, and tested. To benefit from the reliability, safety, and cost advantages, this device can be actuated with passive actuators located outside the shaft that enters the body. The device has 9 DOFs and a diameter of 40 mm. Tests have validated the possibility to conserve the configuration of the shaft of a medical instrument to ultimately perform an alternating FTL motion. The accuracy of the shaft is limited as the concentric shafts interrupt the configuration during the advancement phase. Furthermore, the timing belt teeth at the proximal segments can slip for forces above 1.3 N. The performance improves when the device is assisted by manually interacting with the shaft directly as opposed to proximal steering and advancing.

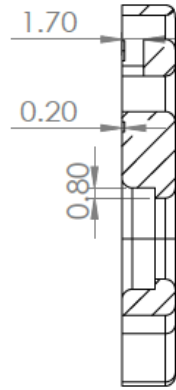
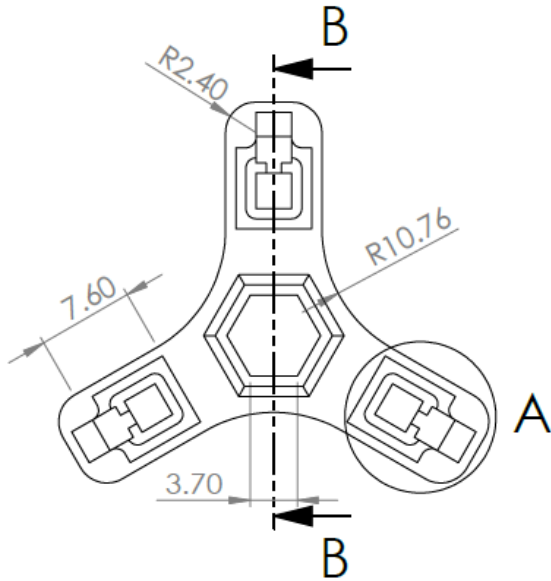
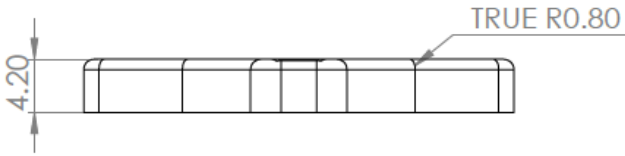
REFERENCES

- [1] A. Bouchard, G. Martel, E. Sabri, E. Poulin, J. Mamazza, and R. Boushey, "Impact of incision length on the short-term outcomes of laparoscopic colorectal surgery," *Surgical endoscopy*, vol. 23, pp. 2314–20, 03 2009.
- [2] K. Mohiuddin and S. Swanson, "Maximizing the benefit of minimally invasive surgery," *Journal of surgical oncology*, vol. 108, 10 2013.
- [3] K. E. Georgeson and D. J. Robertson, "Minimally invasive surgery in the neonate: review of current evidence," *Seminars in Perinatology*, vol. 28, no. 3, pp. 212 – 220, 2004.
- [4] T. Xu, S. M. Hutfless, M. A. Cooper, M. Zhou, A. B. Massie, and M. A. Makary, "Hospital Cost Implications of Increased Use of Minimally Invasive Surgery," *JAMA Surgery*, vol. 150, pp. 489–490, 05 2015.
- [5] "Minimally Invasive Surgery at the Center for Children's Surgery", Accessed on: Mar. 23, 2021. [Online]. Available: <https://www.childrenscolorado.org/doctors-and-departments/departments/surgery/services-we-offer/minimally-invasive-surgery/>.
- [6] B. Kirshtein and E. Haas, "Single port laparoscopic surgery: Concept and controversies of new technique," *Minimally Invasive Surgery*, vol. 2012, 11 2012.
- [7] G. Rao, M. Mansard, P. Ravula, P. Rebala, R. Dama, and D. Reddy, "Single-port surgery: Current applications and limitations," *Asian Journal of Endoscopic Surgery*, vol. 2, no. 3, pp. 56–64, 2009.
- [8] S. Atallah, B. Martin-Perez, D. Keller, J. Burke, and L. Hunter, "Natural-orifice transluminal endoscopic surgery," *British Journal of Surgery*, vol. 102, pp. e73–e92, 01 2015.
- [9] B. M. Shrestha, "Natural orifice transluminal endoscopic surgery (notes): an emerging technique in surgery.," *J Nepal Med Assoc*, vol. 51, pp. 209–212, 2011.
- [10] E. A. Arkenbout, P. W. J. Henselmans, F. Jelinek, and P. Breedveld, "A state of the art review and categorization of multi-branched instruments for notes and sils," *Surgical Endoscopy*, vol. 29, no. 6, pp. 1281–1296, 2015.
- [11] B. A. Koutenaie, E. Wilson, R. Monfaredi, C. Peters, G. Kronreif, and K. Cleary, "Robotic natural orifice transluminal endoscopic surgery (r-notes): Literature review and prototype system," *Minimally Invasive Therapy & Allied Technologies*, vol. 24, no. 1, pp. 18–23, 2015.
- [12] A. Y. Tsai and D. J. Selzer, "Single-port laparoscopic surgery," *Advances in Surgery*, vol. 44, no. 1, pp. 1–27, 2010. *Advances in Surgery*.
- [13] W. Xiaona and M. Meng, "Robotics for natural orifice transluminal endoscopic surgery: A review," *Journal of Robotics*, vol. 2012, 12 2012.
- [14] J. H. Chandler, F. Mushtaq, B. Moxley-Wyles, N. P. West, G. W. Taylor, and P. R. Culmer, "Real-time assessment of mechanical tissue trauma in surgery," *IEEE Transactions on Biomedical Engineering*, vol. 64, pp. 2384–2393, Oct 2017.
- [15] C. Culmone, F. S. Yikilmaz, F. Trauzettel, and P. Breedveld, "Follow-the-leader mechanisms in medical devices: A review on scientific and patent literature," *Literature Study TU Delft BME*, 2021.
- [16] J. Burgner-Kahrs, D. C. Rucker, and H. Choset, "Continuum robots for medical applications: A survey," *IEEE Transactions on Robotics*, vol. 31, pp. 1261–1280, Dec 2015.
- [17] J. Son, C. Cho, K. Kim, T. Chang, H. Jung, S. Kim, M.-T. Kim, N. Yang, T.-Y. Kim, and D. Sohn, "A novel semi-automatic snake robot for natural orifice transluminal endoscopic surgery: preclinical tests in animal and human cadaver models (with video)," *Surgical Endoscopy*, vol. 29, no. 6, pp. 1643–1647, 2015.
- [18] D. Palmer, S. Cobos-Guzman, and D. Axinte, "Real-time method for tip following navigation of continuum snake arm robots," *Robotics and Autonomous Systems*, vol. 62, no. 10, pp. 1478–1485, 2014. cited By 25.
- [19] S. Tappe, J. Pohlmann, J. Kotlarski, and T. Ortmaier, "Towards a follow-the-leader control for a binary actuated hyper-redundant manipulator," vol. 2015-December, pp. 3195–3201, Institute of Electrical and Electronics Engineers Inc., 2015.
- [20] K. Ikuta, M. Tsukamoto, and S. Hirose, "Shape memory alloy servo actuator system with electric resistance feedback and application for active endoscope.," pp. 427–430, IEEE, New York, NY, USA, 1988. cited By 290.
- [21] "Iec 60601-1, medical electrical equipment part 1: General requirements for safety and essential performance," 1995. Recommended Reading.
- [22] R. M. Fish and L. A. Geddes, "Conduction of electrical current to and through the human body: a review," *Eplasty*, vol. 9, pp. e44–e44, Oct 2009. 19907637[pmid].
- [23] T.-D. Nguyen and J. Burgner-Kahrs, "A tendon-driven continuum robot with extensible sections," vol. 2015-December, pp. 2130–2135, Institute of Electrical and Electronics Engineers Inc., 2015.
- [24] H. Lee, K. Kim, J. Seo, and D. Sohn, "Natural orifice transluminal endoscopic surgery with a snake-mechanism using a movable pulley," *The International Journal of Medical Robotics and Computer Assisted Surgery*, vol. 13, p. e1816, 03 2017.
- [25] C. P. Childers and M. Maggard-Gibbons, "Estimation of the Acquisition and Operating Costs for Robotic Surgery," *JAMA*, vol. 320, pp. 835–836, 08 2018.
- [26] R. E. Perez and S. D. Schwaitzberg, "Robotic surgery: finding value in 2019 and beyond," *Annals of Laparoscopic and Endoscopic Surgery*, vol. 4, no. 0, 2019.
- [27] N. C. Buchs, F. Pugin, F. Volonté, and P. Morel, "Reliability of robotic system during general surgical procedures in a university hospital," *The American Journal of Surgery*, vol. 207, no. 1, pp. 84–88, 2014.
- [28] S. Lang, S. Mattheis, P. Hasskamp, G. Lawson, C. Güldner, M. Mandapathil, P. Schuler, T. Hoffmann, M. Scheithauer, and M. Remacle, "A european multicenter study evaluating the flex robotic system in transoral robotic surgery," *The Laryngoscope*, vol. 127, no. 2, pp. 391–395, 2017.
- [29] P. Sears and P. Dupont, "A steerable needle technology using curved concentric tubes," pp. 2850–2856, 2006.
- [30] H. Gilbert and R. Webster, "Can concentric tube robots follow the leader?," pp. 4881–4887, 2013.
- [31] J. Burgner-Kahrs, H. B. Gilbert, J. Granna, P. J. Swaney, and R. J. Webster, "Workspace characterization for concentric tube continuum robots," in *2014 IEEE/RSJ International Conference on Intelligent Robots and Systems*, pp. 1269–1275, Sep. 2014.
- [32] E. Butler, R. Hammond-Oakley, S. Chawarski, A. Gosline, P. Codd, T. Anor, J. Madsen, P. Dupont, and J. Lock, "Robotic neuro-endoscope with concentric tube augmentation," pp. 2941–2946, 2012.
- [33] C. Girerd, K. Rabenorosoa, P. Rougeot, and P. Renaud, "Towards optical biopsy of olfactory cells using concentric tube robots with follow-the-leader deployment," vol. 2017-September, pp. 5661–5667, Institute of Electrical and Electronics Engineers Inc., 2017.
- [34] J. Granna, T. Rau, T.-D. Nguyen, T. Lenarz, O. Majdani, and J. Burgner-Kahrs, "Toward automated cochlear implant insertion using tubular manipulators," vol. 9786, SPIE, 2016.
- [35] Y. Gao, K. Takagi, T. Kato, N. Shono, and N. Hata, "Continuum robot with follow-the-leader motion for endoscopic third ventriculostomy and tumor biopsy," *IEEE Transactions on Biomedical Engineering*, vol. 67, no. 2, pp. 379–390, 2020. cited By 1.
- [36] H. M. Choset, A. Wolf, and M. A. Zenati, "Steerable, follow the leader device," Dec. 11 2018. U.S. Patent 10 149 607.
- [37] P. Henselmans, G. Smit, and P. Breedveld, "Mechanical follow-the-leader motion of a hyper-redundant surgical instrument: Proof-of-concept prototype and first tests," *Proceedings of the Institution of Mechanical Engineers, Part H: Journal of Engineering in Medicine*, vol. 233, no. 11, pp. 1141–1150, 2019.
- [38] "Flex® Robotic System: expanding the reach of surgery®", Accessed on: Mar. 3, 2020. [Online]. Available: <https://www.medrobotics.com/gateway/flex-system-int/>.
- [39] B. Kang, R. Kojev, and E. Sinibaldi, "The first interlaced continuum robot, devised to intrinsically follow the leader," *PLoS ONE*, vol. 11, no. 2, 2016.
- [40] V. Saadat, R. C. Ewers, and E. G. Chen, "Shape lockable apparatus and method for advancing an instrument through unsupported anatomy," June 23 2005. U.S. Patent 0 137 456.
- [41] A. Loeve, P. Breedveld, and J. Dankelman, "Scopes too flexible...and too stiff," *Pulse, IEEE*, vol. 1, pp. 26 – 41, 01 2011.
- [42] L. Blanc, A. Pol, B. François, A. Delchambre, P. Lambert, and F. Gabrieli, "Granular jamming as controllable stiffness mechanism for medical devices," in *Micro to MACRO Mathematical Modelling in Soil Mechanics* (P. Giovine, P. M. Mariano, and G. Mortara, eds.), (Cham), pp. 57–66, Springer International Publishing, 2018.
- [43] N. G. Cheng, M. B. Lobovsky, S. J. Keating, A. M. Setapen, K. I. Gero, A. E. Hosoi, and K. D. Iagnemma, "Design and analysis of a robust, low-cost, highly articulated manipulator enabled by jamming of granular media," in *2012 IEEE International Conference on Robotics and Automation*, pp. 4328–4333, May 2012.
- [44] K. Ikuta, Y. Matsuda, D. Yajima, and Y. Ota, "Pressure pulse drive: A control method for the precise bending of hydraulic active catheters," *IEEE/ASME Transactions on Mechatronics*, vol. 17, pp. 876–883, Oct 2012.

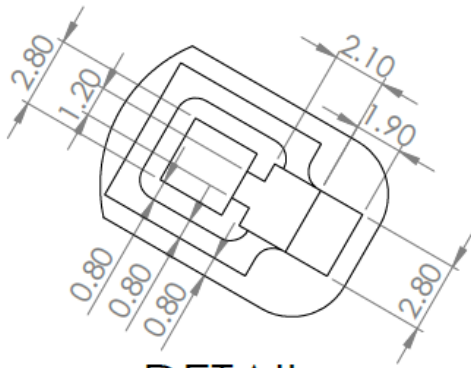
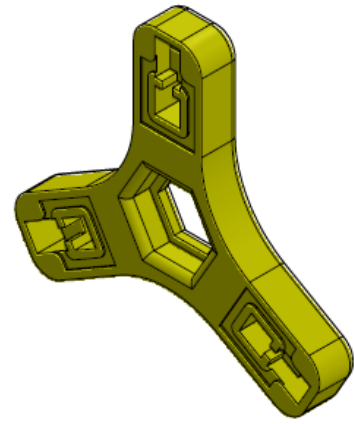
- [45] A. Yagi, K. Matsumiya, K. Masamune, H. Liao, and T. Dohi, *Rigid-flexible outer sheath model using shape lock mechanism by air pressure and wire driven curving mechanism*, vol. 14, pp. 3108–3111. 01 2007.
- [46] T. Seah, T. N. Do, N. Takeshita, K. Ho, and S. Phee, “Future of flexible robotic endoscopy systems,” 03 2017.
- [47] G. Ciuti, K. Skonieczna-Żydecka, W. Marlicz, V. Iacovacci, H. Liu, D. Stoyanov, A. Arezzo, M. Chiurazzi, E. Toth, H. Thorlacius, P. Dario, and A. Koulaouzidis, “Frontiers of robotic colonoscopy: A comprehensive review of robotic colonoscopes and technologies,” *Journal of Clinical Medicine*, vol. 9, no. 6, 2020.
- [48] Y. Chen, J. Chang, A. Greenlee, K. Cheung, A. Slocum, and R. Gupta, “Multi-turn, tension-stiffening catheter navigation system,” pp. 5570–5575, 2010. cited By 21.
- [49] I. G. Jeong, Y. S. Khandwala, J. H. Kim, D. H. Han, S. Li, Y. Wang, S. L. Chang, and B. I. Chung, “Association of Robotic-Assisted vs Laparoscopic Radical Nephrectomy With Perioperative Outcomes and Health Care Costs, 2003 to 2015,” *JAMA*, vol. 318, pp. 1561–1568, 10 2017.
- [50] R. E. Perez and S. D. Schwaitzberg, “Robotic surgery: finding value in 2019 and beyond,” *Annals of Laparoscopic and Endoscopic Surgery*, vol. 4, no. 0, 2019.
- [51] “Synchromesh Drive Systems”, Accessed on: Mar. 25, 2020. [Online]. Available: <https://www.sdp-si.com/products/Timing-Belts-and-Cables/Synchromesh-Drive-Systems.php>.
- [52] A. Vasan and J. Friend, “Medical devices for low and middle income countries: A review and directions for development,” *Journal of Medical Devices*, vol. 14, 03 2020.
- [53] R. Lilford, S. Burn, K. Diaconu, P. Lilford, P. Chilton, V. Bion, C. Cummins, and S. Manaseki-Holland, “An approach to prioritization of medical devices in low-income countries: An example based on the republic of south sudan,” *Cost effectiveness and resource allocation : C/E*, vol. 13, p. 2, 12 2015.
- [54] R. A. Malkin, “Barriers for medical devices for the developing world,” *Expert Review of Medical Devices*, vol. 4, no. 6, pp. 759–763, 2007.

APPENDIX

A. Engineering drawings

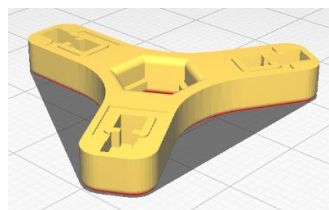


SECTION B-B

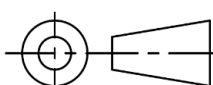



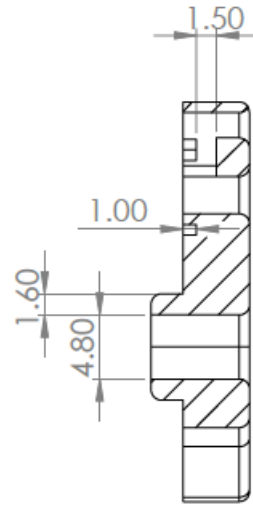
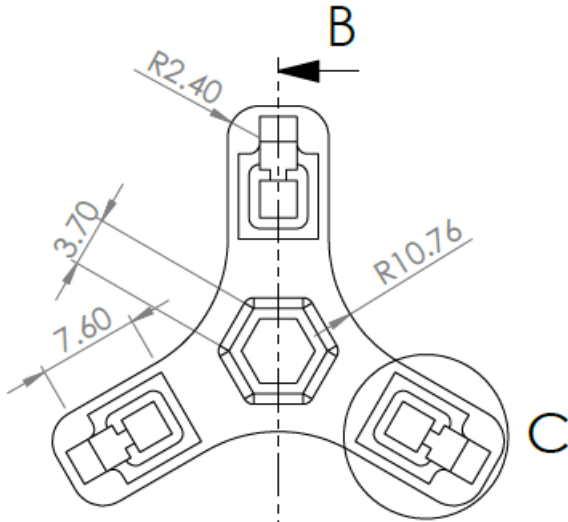
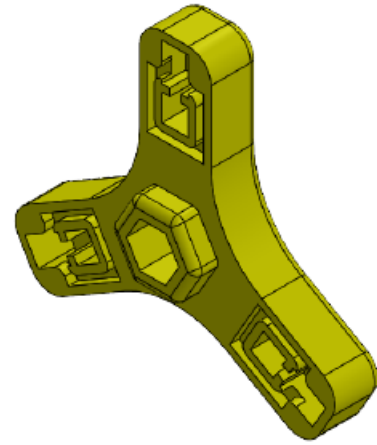
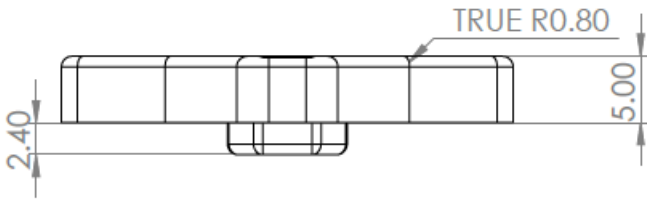
DETAIL A

SCALE 4 : 1

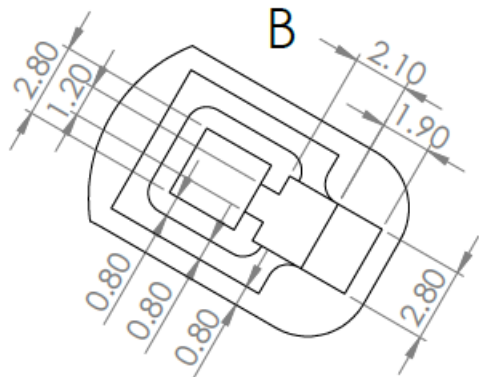


3D printer:	
Creality Ender 3	
Slicer:	
Ultimaker Cura 4.8.0	
Print setting	
Temperature	195°C
Layer height	0.2 mm
Print speed	50.0 mm/s
Support	None
Build plate Adhesion	Skirt

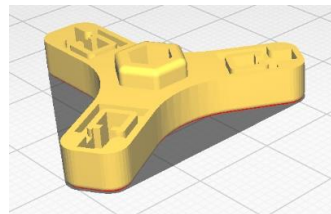
ROUGHNESS:	FINISH:	MATERIAL: PLA (Jupiter serie; 123-3D.nl)	MASS [g]:
THIRD ANGLE PROJECTION 	SCALE: 2:1 DIMENSION: mm DATE: 31-03-2021	DRAWN AND DESIGNED BY: NAME: Fatih Semih Yikilmaz STUDENT NUMBER: 4373634 E-MAIL: F.S.Yikilmaz@student.tudelft.nl	
	Biomechanical Engineering (BME)	NAME/DESCRIPTION: Inner-shaft segment disk (female)	A4



SECTION B-B

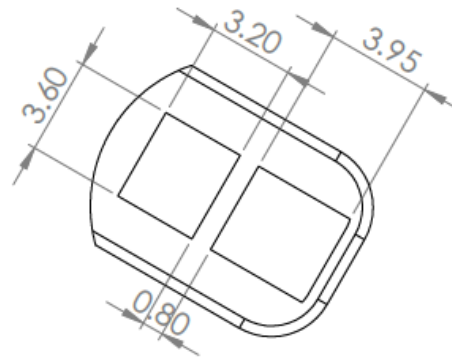
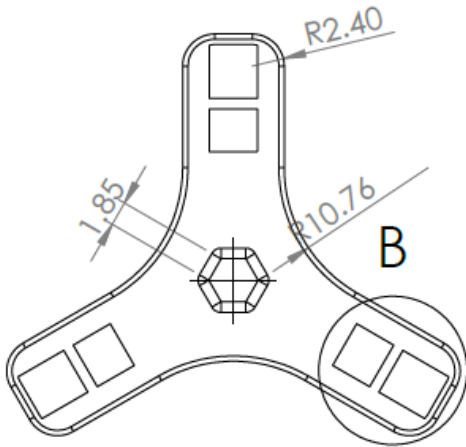
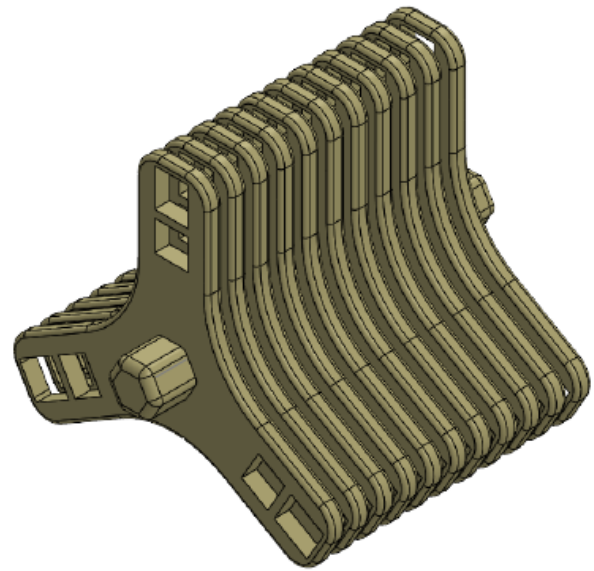
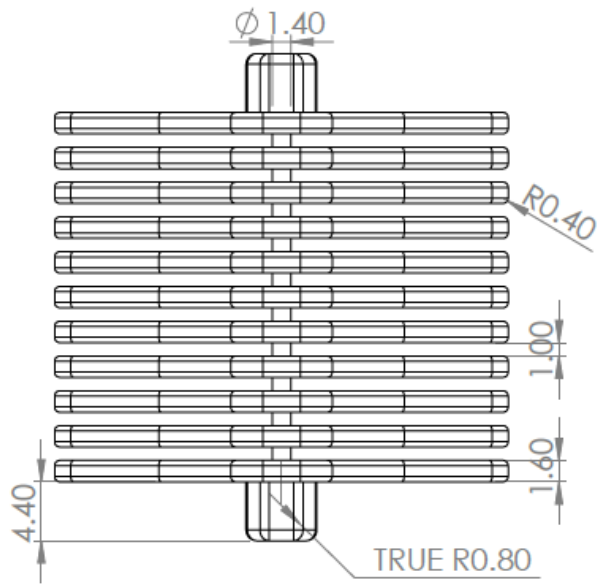


DETAIL C
SCALE 4 : 1

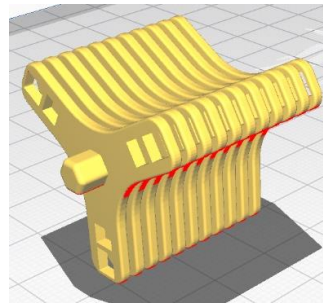


3D printer:	
Creality Ender 3	
Slicer:	
Ultimaker Cura 4.8.0	
Print setting	
Temperature	195°C
Layer height	0.2 mm
Print speed	50.0 mm/s
Support	None
Build plate	Skirt
Adhesion	

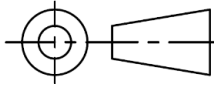

ROUGHNESS:	FINISH:	MATERIAL: PLA (Jupiter serie; 123-3D.nl)	MASS [g]:
<small>THIRD ANGLE PROJECTION</small> 	SCALE: 2:1	DRAWN AND DESIGNED BY: NAME: Fatih Semih Yikilmaz STUDENT NUMBER: 4373634 E-MAIL: F.S.Yikilmaz@student.tudelft.nl	
	DIMENSION: mm		
	DATE: 31-03-2021		
	Biomechanical Engineering (BME)	NAME/DESCRIPTION: Inner-shaft segment disk (male)	A4

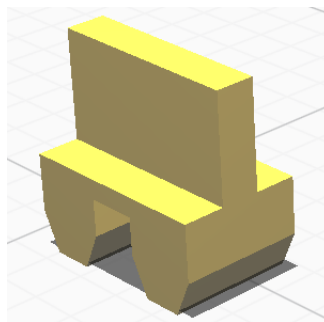
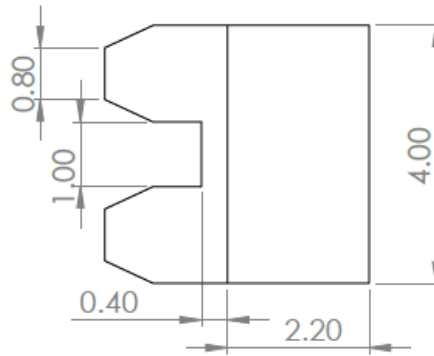
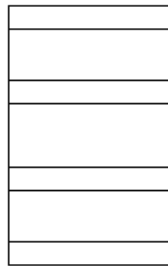
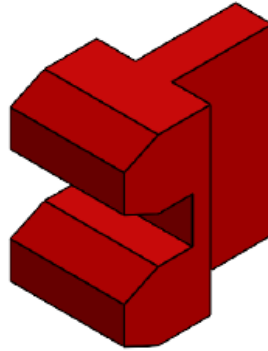
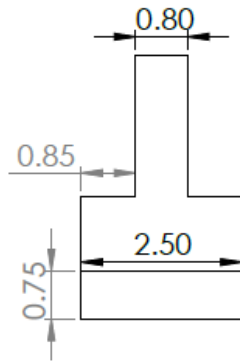


DETAIL B
SCALE 4 : 1

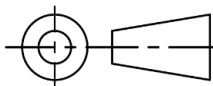



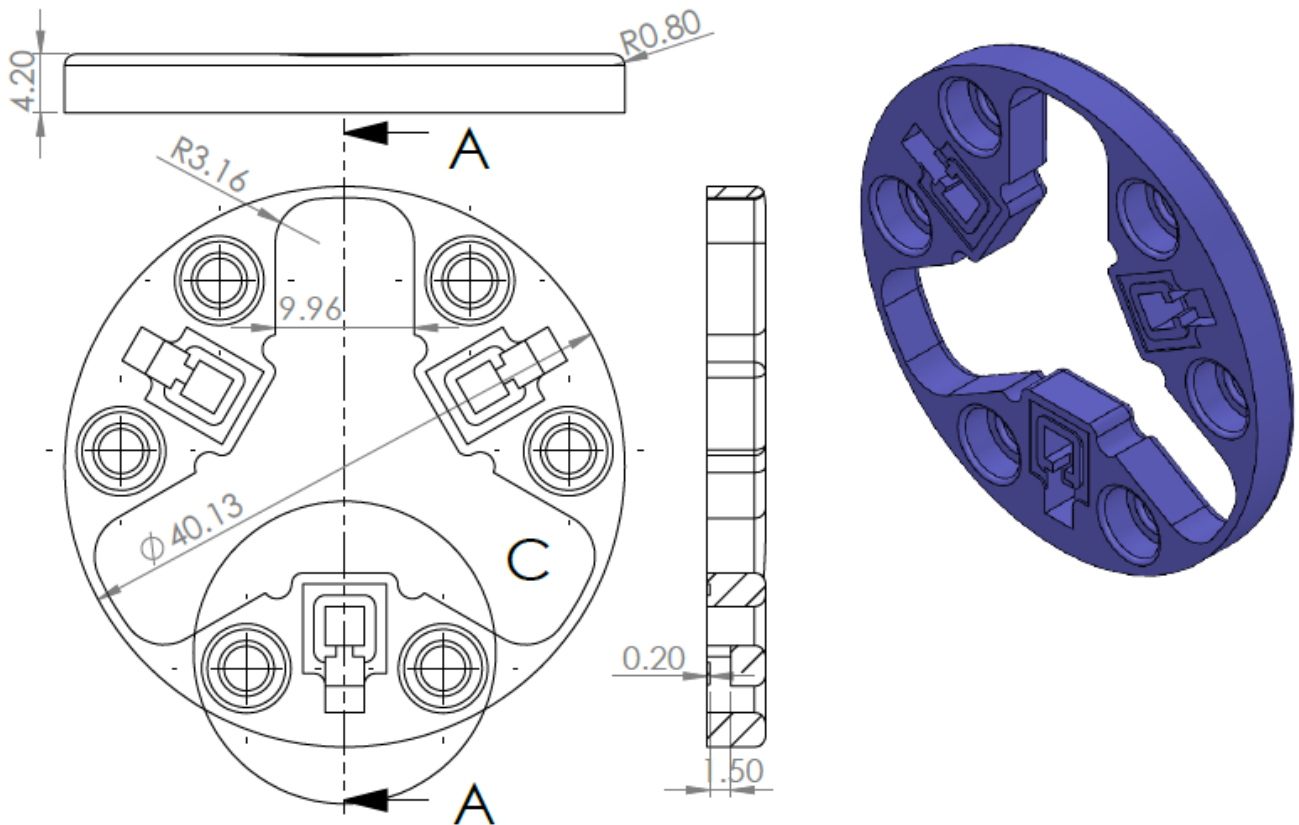
3D printer:	
Creality Ender 3	
Slicer:	
Ultimaker Cura 4.8.0	
Print setting	
Temperature	195°C
Layer height	0.2 mm
Print speed	50.0 mm/s
Support	Touching build plate
Build plate Adhesion	Brim

ROUGHNESS:	FINISH:	MATERIAL: PLA (Jupiter serie; 123-3D.nl)	MASS [g]:
THIRD ANGLE PROJECTION 	SCALE: 2:1 DIMENSION: mm DATE: 31-03-2021	DRAWN AND DESIGNED BY: NAME: Fatih Semih Yikilmaz STUDENT NUMBER: 4373634 E-MAIL: F.S.Yikilmaz@student.tudelft.nl	
	Biomechanical Engineering (BME)	NAME/DESCRIPTION: Inner-shaft segment joint	A4

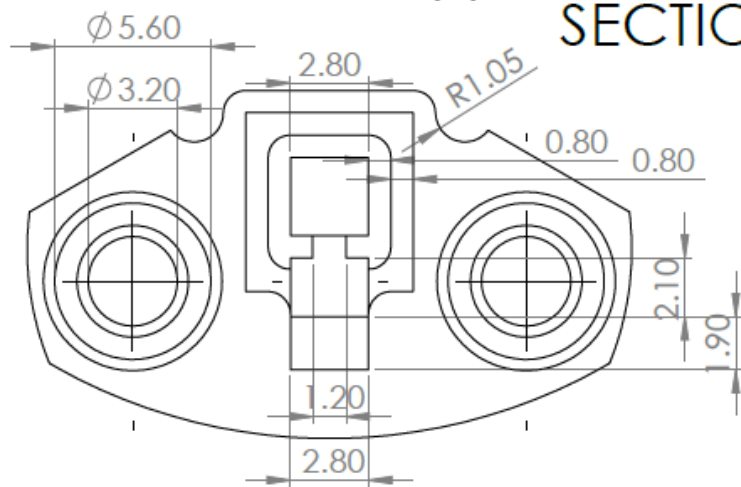


3D printer:	
Creality Ender 3	
Slicer:	
Ultimaker Cura 4.8.0	
Print setting	
Temperature	195°C
Layer height	0.1 mm
Print speed	20.0 mm/s
Support	None
Build plate	None
Adhesion	

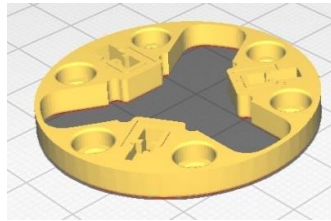
ROUGHNESS:	FINISH:	MATERIAL: PLA (Jupiter serie; 123-3D.nl)	MASS [g]:
THIRD ANGLE PROJECTION 	SCALE: 10:1 DIMENSION: mm DATE: 31-03-2021	DRAWN AND DESIGNED BY: NAME: Fatih Semih Yikilmaz STUDENT NUMBER: 4373634 E-MAIL: F.S.Yikilmaz@student.tudelft.nl	
	Biomechanical Engineering (BME)	NAME/DESCRIPTION: Stopper	A4



SECTION A-A

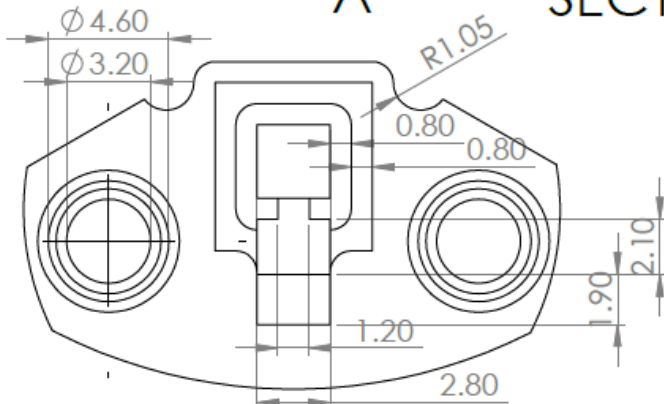
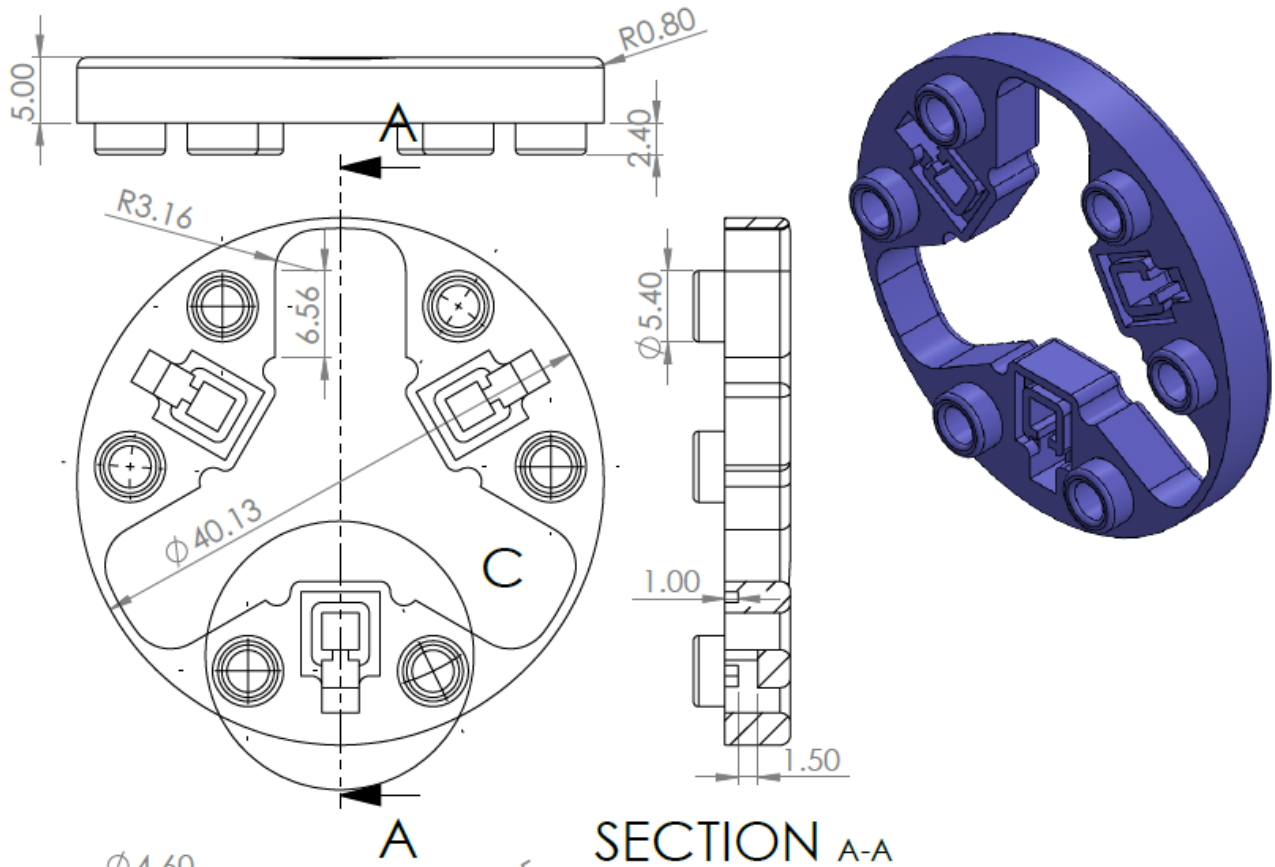


DETAIL C
SCALE 4 : 1

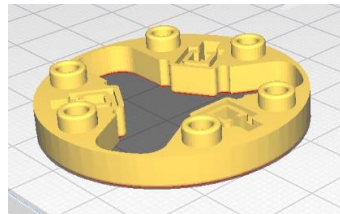


3D printer:		Creality Ender 3	
Slicer:		Ultimaker Cura 4.8.0	
Print setting			
Temperature		195°C	
Layer height		0.2 mm	
Print speed		50.0 mm/s	
Support		None	
Build plate		Skirt	
Adhesion			

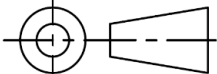

ROUGHNESS:	FINISH:	MATERIAL: PLA (Jupiter serie; 123-3D.nl)	MASS [g]:
THIRD ANGLE PROJECTION 	SCALE: 2:1	DRAWN AND DESIGNED BY:	
	DIMENSION: mm	NAME: Fatih Semih Yikilmaz	
	DATE: 31-03-2021	STUDENT NUMBER: 4373634	
	Biomechanical Engineering (BME)	E-MAIL: F.S.Yikilmaz@student.tudelft.nl	
		NAME/DESCRIPTION: Outer-shaft segment disk (female)	A4

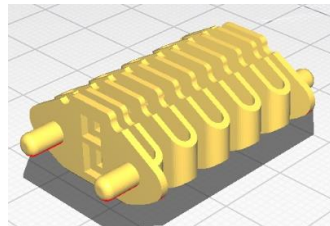
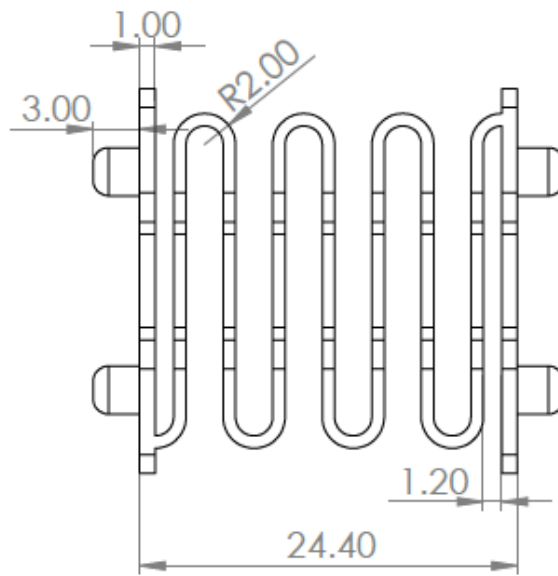
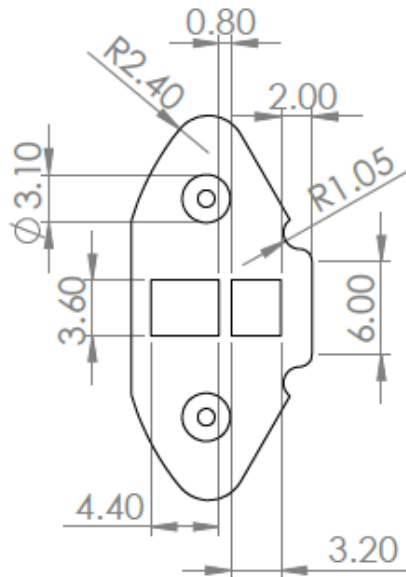
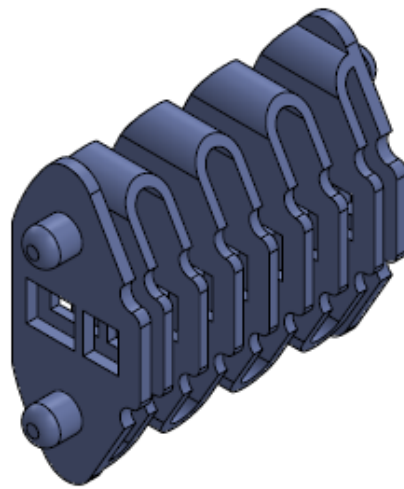


DETAIL C
SCALE 4 : 1



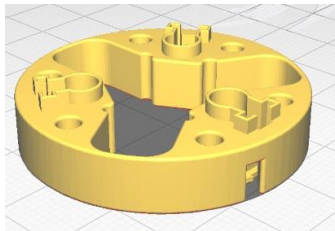
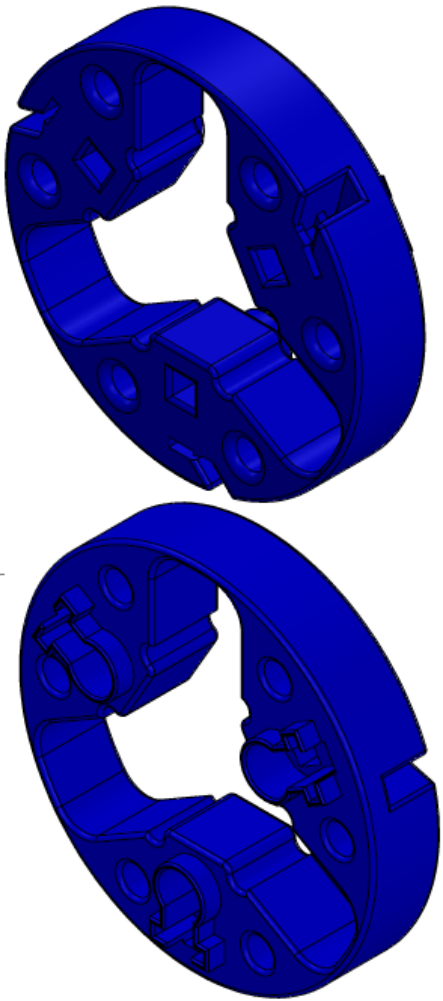
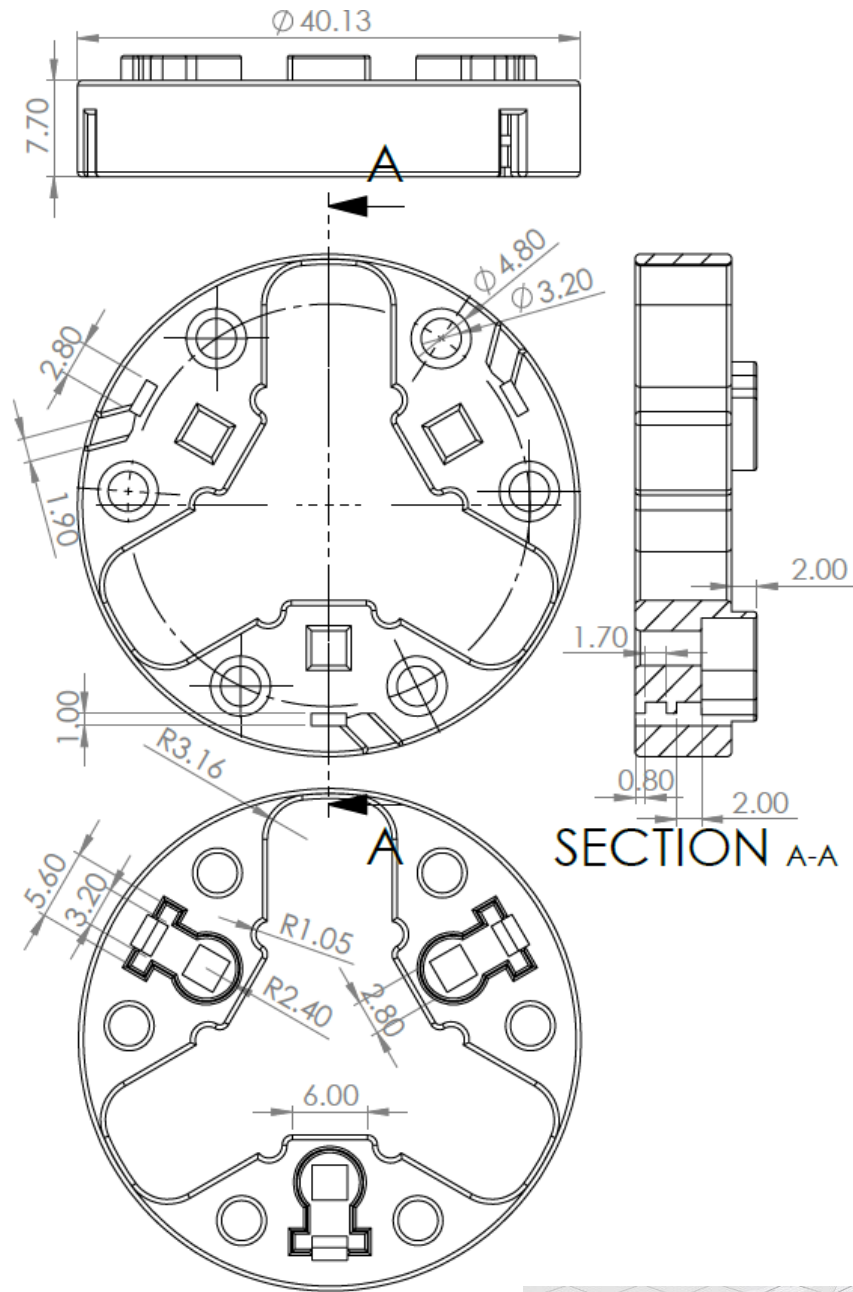
3D printer:	
Creality Ender 3	
Slicer:	
Ultimaker Cura 4.8.0	
Print setting	
Temperature	195°C
Layer height	0.2 mm
Print speed	50.0 mm/s
Support	None
Build plate Adhesion	Skirt

ROUGHNESS:	FINISH:	MATERIAL: PLA (Jupiter serie; 123-3D.nl)	MASS [g]:
THIRD ANGLE PROJECTION 	SCALE: 2:1 DIMENSION: mm DATE: 31-03-2021	DRAWN AND DESIGNED BY: NAME: Fatih Semih Yikilmaz STUDENT NUMBER: 4373634 E-MAIL: F.S.Yikilmaz@student.tudelft.nl	
	Biomechanical Engineering (BME)	NAME/DESCRIPTION: Outer-shaft segment disk (male)	A4

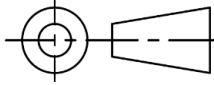



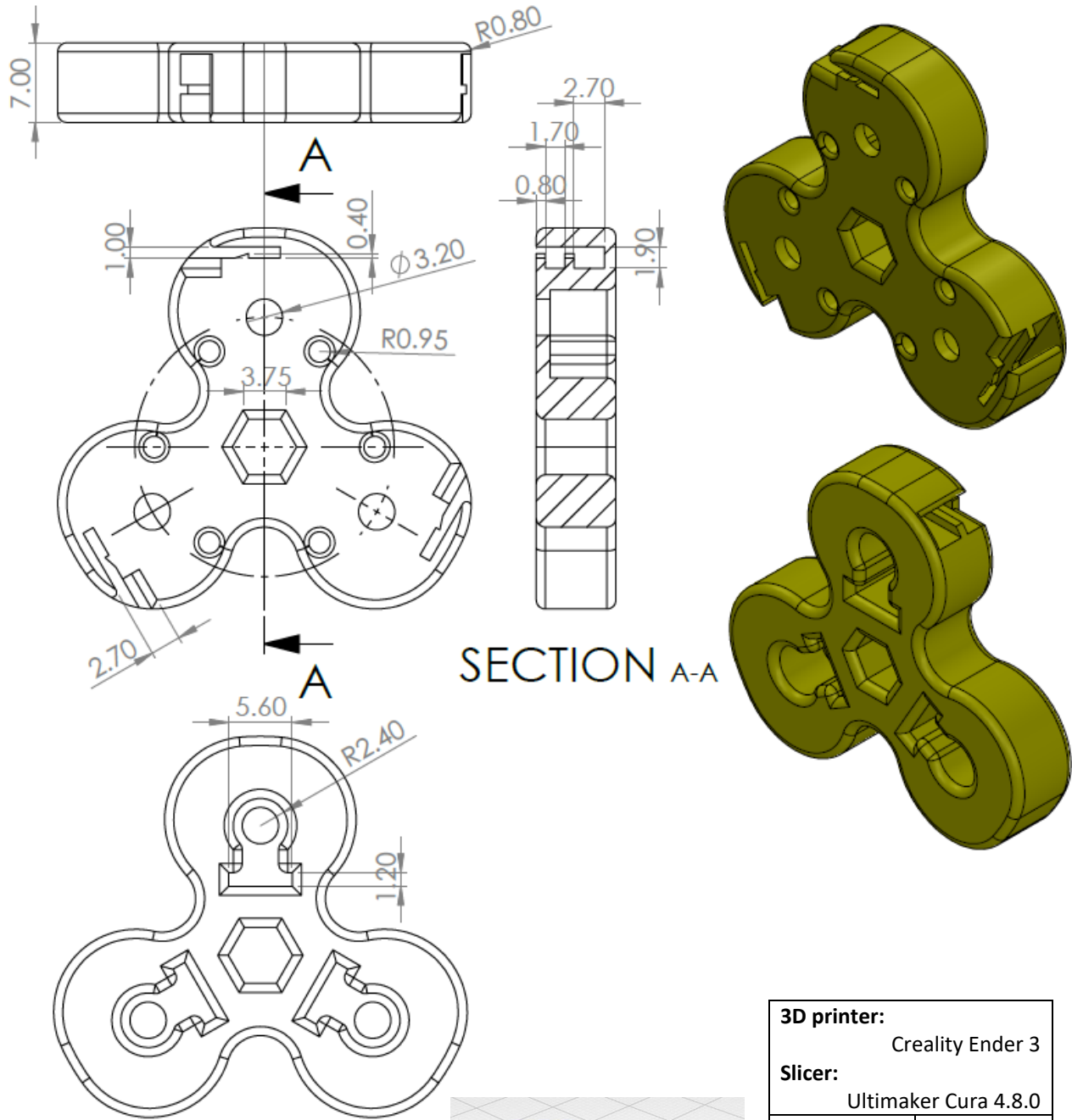
3D printer:		Creality Ender 3	
Slicer:		Ultimaker Cura 4.8.0	
Print setting			
Temperature	195°C		
Layer height	0.2 mm		
Print speed	50.0 mm/s		
Support	Touching build plate		
Build plate Adhesion	Brim		

ROUGHNESS:	FINISH:	MATERIAL: PLA (Jupiter serie; 123-3D.nl)	MASS [g]:
THIRD ANGLE PROJECTION 	SCALE: 2:1	DRAWN AND DESIGNED BY: NAME: Fatih Semih Yikilmaz STUDENT NUMBER: 4373634 E-MAIL: F.S.Yikilmaz@student.tudelft.nl	
	DIMENSION: mm		
	DATE: 31-03-2021		
	Biomechanical Engineering (BME)	NAME/DESCRIPTION: Outer-shaft segment joint	A4

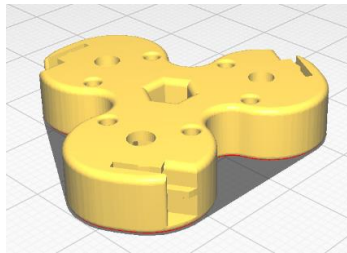


3D printer:		Creality Ender 3	
Slicer:		Ultimaker Cura 4.8.0	
Print setting			
Temperature		195°C	
Layer height		0.2 mm	
Print speed		50.0 mm/s	
Support		None	
Build plate		Skirt	
Adhesion			

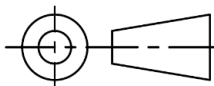

ROUGHNESS:	FINISH:	MATERIAL: PLA (Jupiter serie; 123-3D.nl)	MASS [g]:
THIRD ANGLE PROJECTION 	SCALE: 2:1 DIMENSION: mm DATE: 31-03-2021	DRAWN AND DESIGNED BY: NAME: Fatih Semih Yikilmaz STUDENT NUMBER: 4373634 E-MAIL: F.S.Yikilmaz@student.tudelft.nl	
 TU Delft	Biomechanical Engineering (BME)	NAME/DESCRIPTION: Outer-shaft end-effector disk	A4

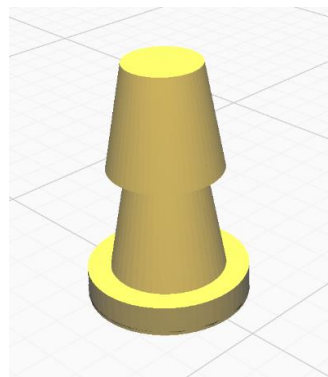
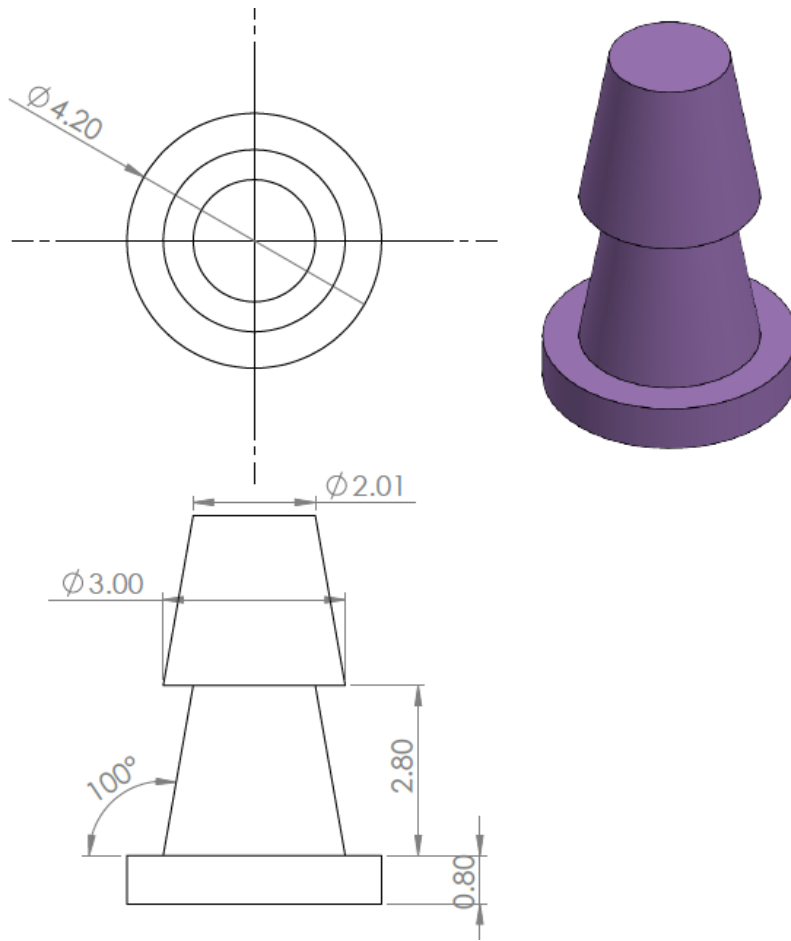


SECTION A-A



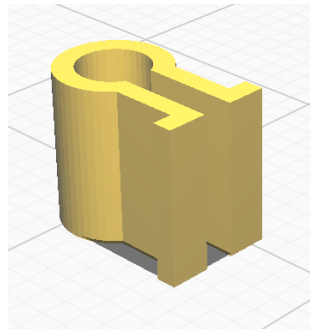
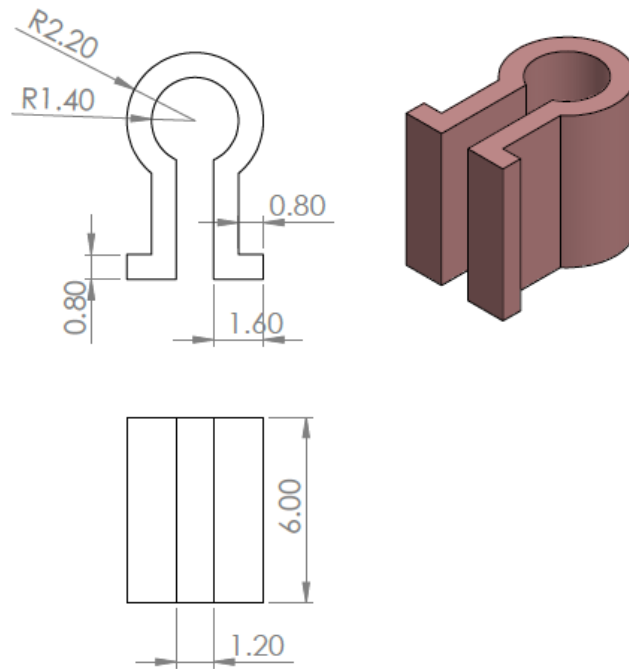
3D printer:		Creality Ender 3	
Slicer:		Ultimaker Cura 4.8.0	
Print setting			
Temperature		195°C	
Layer height		0.2 mm	
Print speed		50.0 mm/s	
Support		None	
Build plate		Skirt	
Adhesion			

ROUGHNESS:	FINISH:	MATERIAL: PLA (Jupiter serie; 123-3D.nl)	MASS [g]:
THIRD ANGLE PROJECTION 	SCALE: 2:1 DIMENSION: mm DATE: 31-03-2021	DRAWN AND DESIGNED BY: NAME: Fatih Semih Yikilmaz STUDENT NUMBER: 4373634 E-MAIL: F.S.Yikilmaz@student.tudelft.nl	
 TU Delft	Biomechanical Engineering (BME)	NAME/DESCRIPTION: Inner-shaft end-effector disk	A4

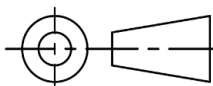



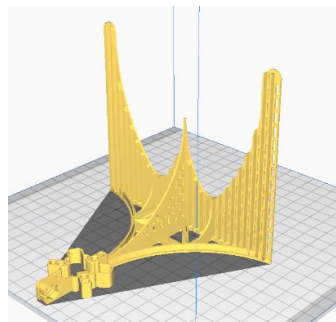
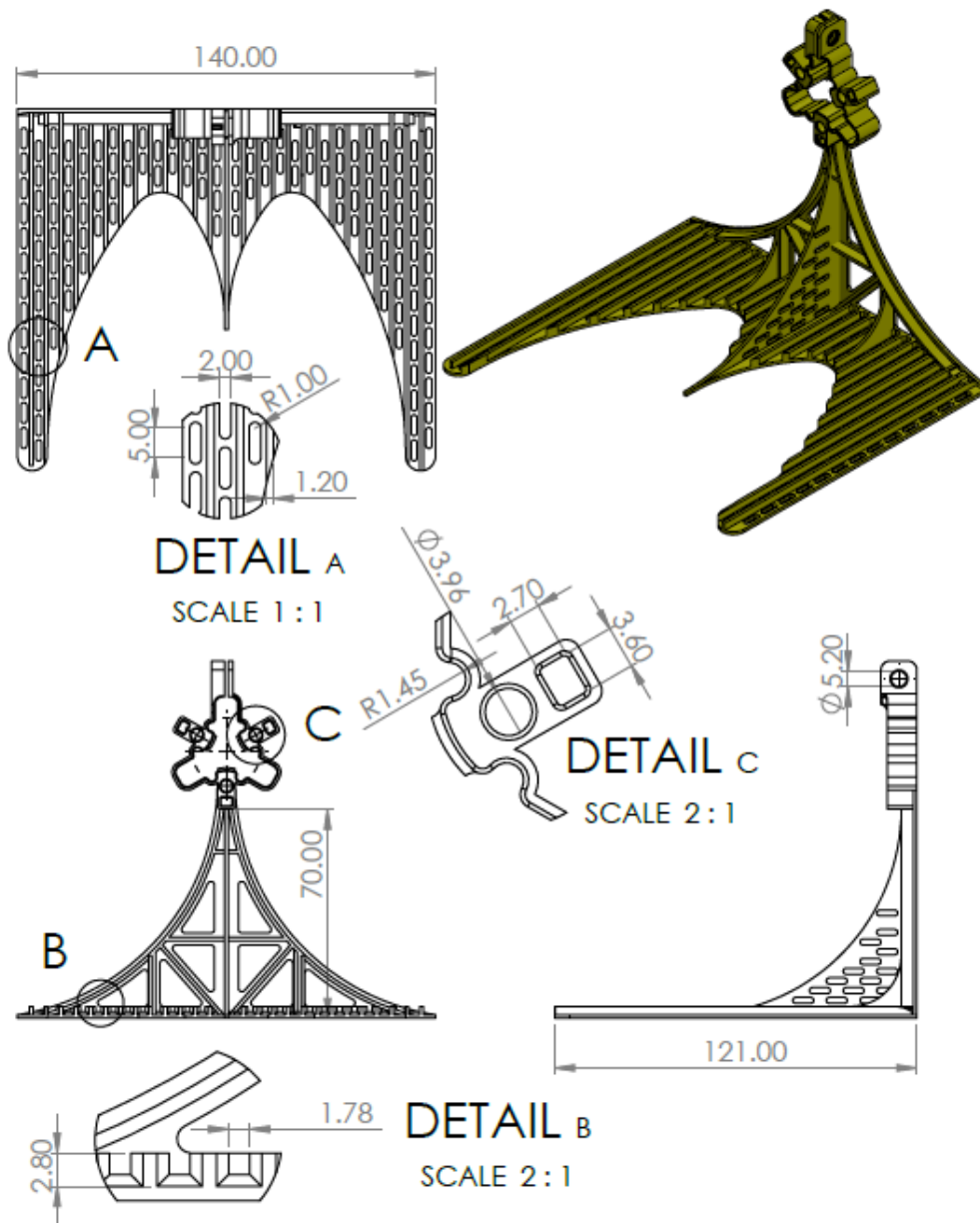
3D printer:	
Creality Ender 3	
Slicer:	
Ultimaker Cura 4.8.0	
Print setting	
Temperature	195°C
Layer height	0.1 mm
Print speed	50.0 mm/s
Support	None
Build plate	Brim
Adhesion	

ROUGHNESS:	FINISH:	MATERIAL: PLA (Jupiter serie; 123-3D.nl)	MASS [g]:
THIRD ANGLE PROJECTION 	SCALE: 10:1 DIMENSION: mm DATE: 31-03-2021	DRAWN AND DESIGNED BY: NAME: Fatih Semih Yikilmaz STUDENT NUMBER: 4373634 E-MAIL: F.S.Yikilmaz@student.tudelft.nl	
	Biomechanical Engineering (BME)	NAME/DESCRIPTION: Pneumatic tube plug	A4

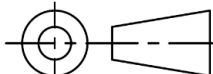



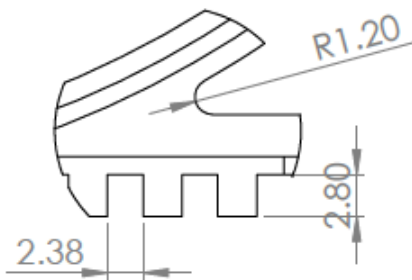
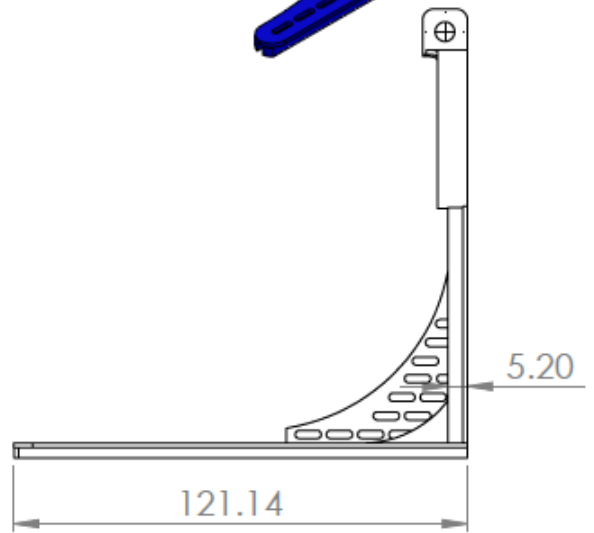
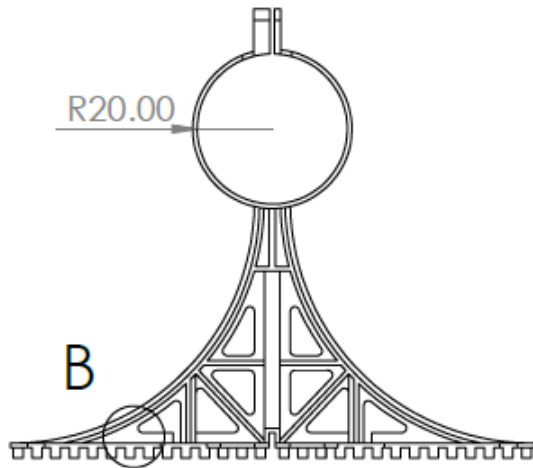
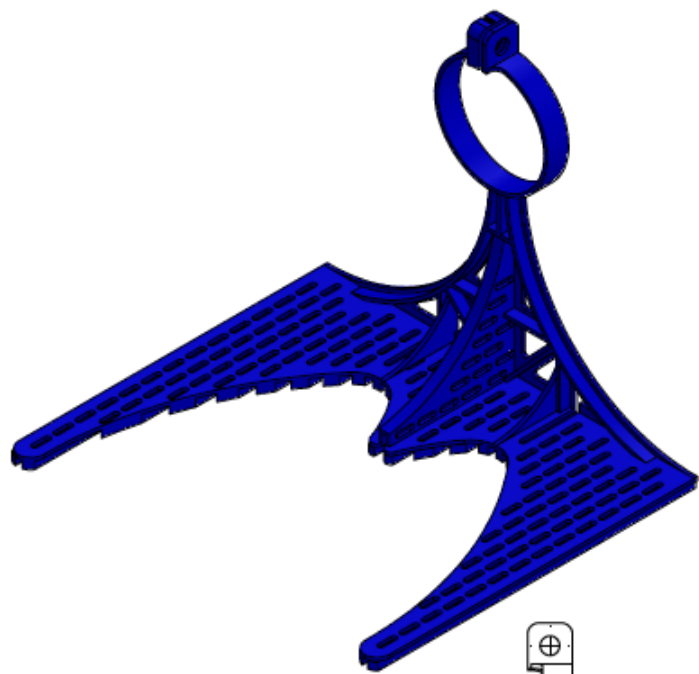
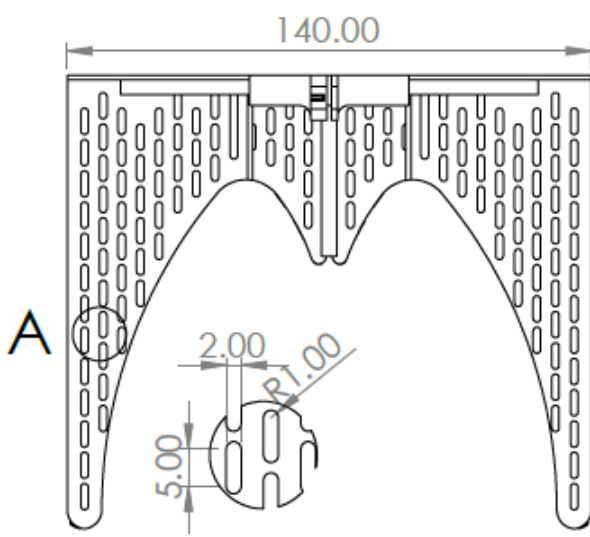
3D printer:		Crealty Ender 3
Slicer:		Ultimaker Cura 4.8.0
Print setting		
Temperature		195°C
Layer height		0.1 mm
Print speed		50.0 mm/s
Support		None
Build plate Adhesion		Brim

ROUGHNESS:	FINISH:	MATERIAL: PLA (Jupiter serie; 123-3D.nl)	MASS [g]:
THIRD ANGLE PROJECTION 	SCALE: 10:1	DRAWN AND DESIGNED BY:	
	DIMENSION: mm	NAME: Fatih Semih Yikilmaz	
	DATE: 31-03-2021	STUDENT NUMBER: 4373634	
	Biomechanical Engineering (BME)	E-MAIL: F.S.Yikilmaz@student.tudelft.nl	
		NAME/DESCRIPTION: Pneumatic tube clamp	A4

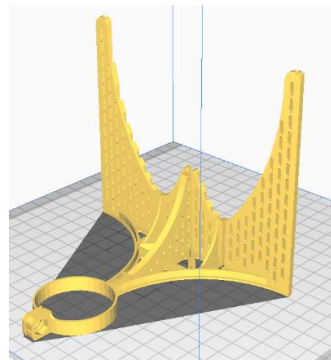


3D printer:	Crealitty Ender 3
Slicer:	Ultimaker Cura 4.8.0
Print setting	
Temperature	195°C
Layer height	0.28 mm
Print speed	50.0 mm/s
Support	None
Build plate	Skirt
Adhesion	

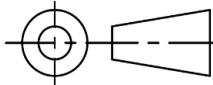

ROUGHNESS:	FINISH:	MATERIAL: PLA (Jupiter serie; 123-3D.nl)	MASS [g]:
THIRD ANGLE PROJECTION 	SCALE: 1:2	DRAWN AND DESIGNED BY: NAME: Fatih Semih Yikilmaz	
	DIMENSION: mm	STUDENT NUMBER: 4373634	
	DATE: 31-03-2021	E-MAIL: F.S.Yikilmaz@student.tudelft.nl	
	Biomechanical Engineering (BME)	NAME/DESCRIPTION: Inner-shaft stand	A4

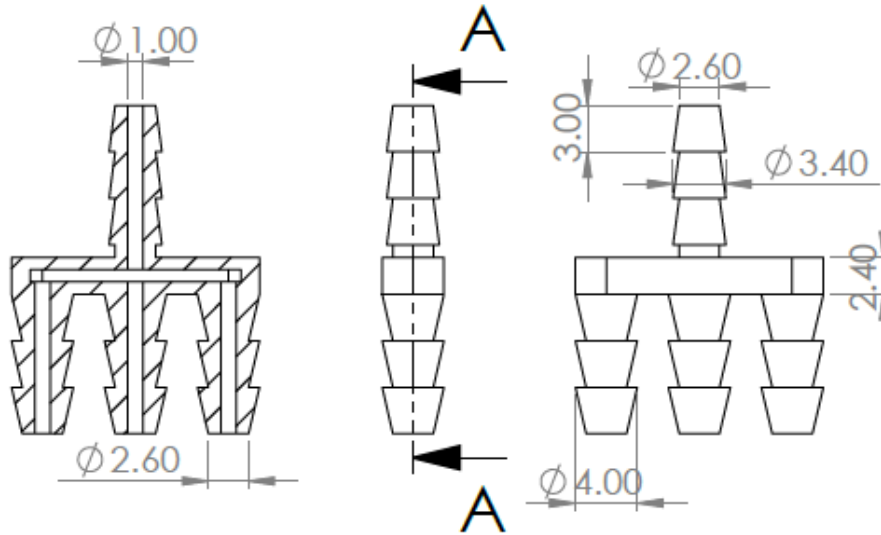
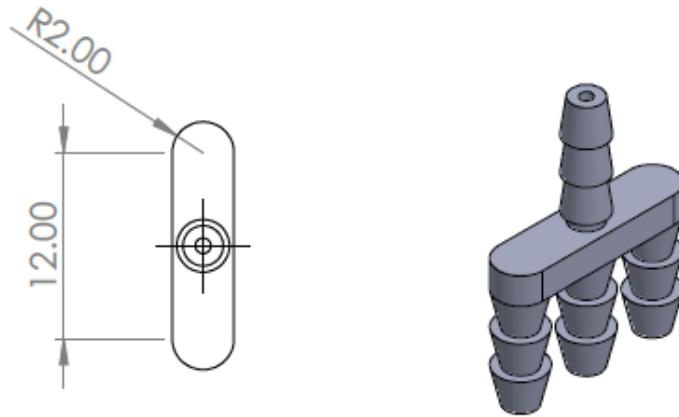


DETAIL B
SCALE 2 : 1

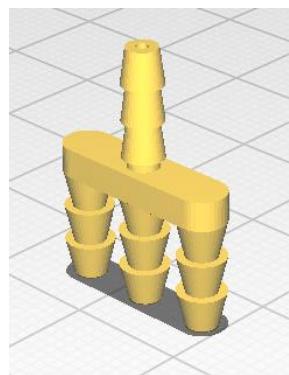


3D printer:	
Creality Ender 3	
Slicer:	
Ultimaker Cura 4.8.0	
Print setting	
Temperature	195°C
Layer height	0.28 mm
Print speed	50.0 mm/s
Support	None
Build plate Adhesion	Skirt

ROUGHNESS:	FINISH:	MATERIAL: PLA (Jupiter serie; 123-3D.nl)	MASS [g]:
THIRD ANGLE PROJECTION 	SCALE: 1:2 DIMENSION: mm DATE: 31-03-2021	DRAWN AND DESIGNED BY: NAME: Fatih Semih Yikilmaz STUDENT NUMBER: 4373634 E-MAIL: F.S.Yikilmaz@student.tudelft.nl	
	Biomechanical Engineering (BME)	NAME/DESCRIPTION: Outer-shaft stand	A4

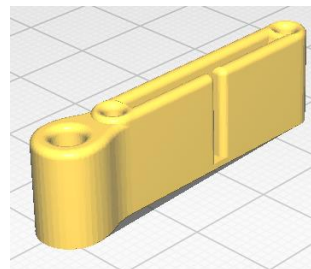
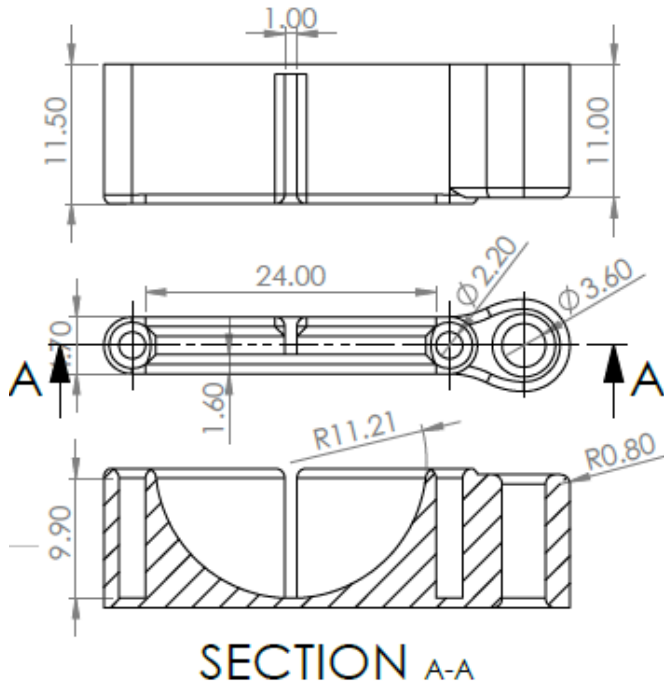
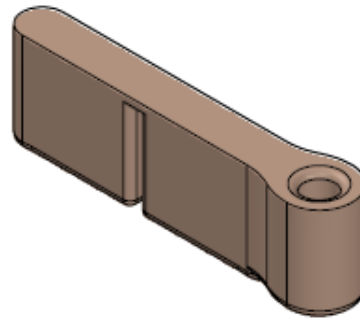


SECTION A-A



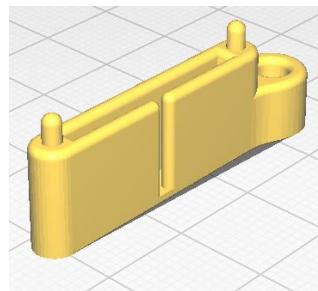
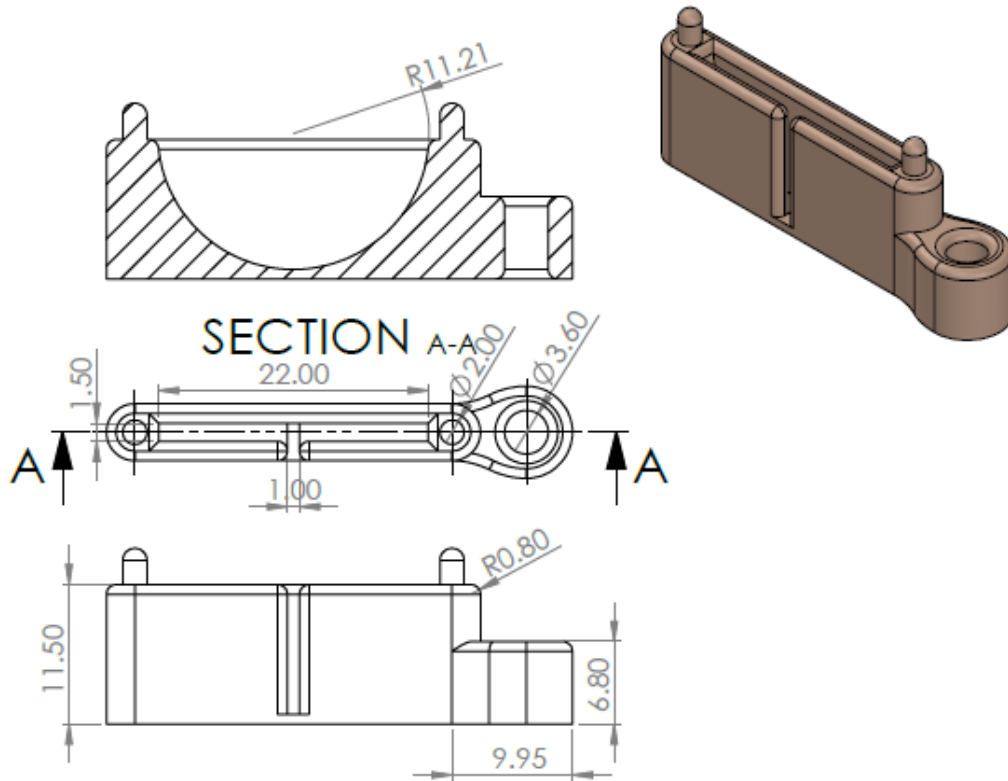
3D printer:	
Creality Ender 3	
Slicer:	
Ultimaker Cura 4.8.0	
Print setting	
Temperature	195°C
Layer height	0.1 mm
Print speed	50.0 mm/s
Support	None
Build plate	Brim
Adhesion	

ROUGHNESS:	FINISH:	MATERIAL: PLA (Jupiter serie; 123-3D.nl)	MASS [g]:
THIRD ANGLE PROJECTION 	SCALE: 2:1	DRAWN AND DESIGNED BY: NAME: Fatih Semih Yikilmaz STUDENT NUMBER: 4373634 E-MAIL: F.S.Yikilmaz@student.tudelft.nl	
	DIMENSION: mm		
	DATE: 31-03-2021		
	Biomechanical Engineering (BME)	NAME/DESCRIPTION: Pneumatic fitting	A4



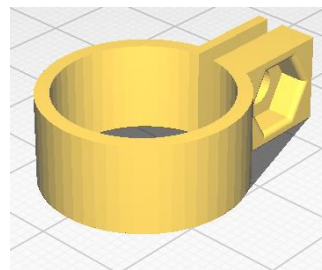
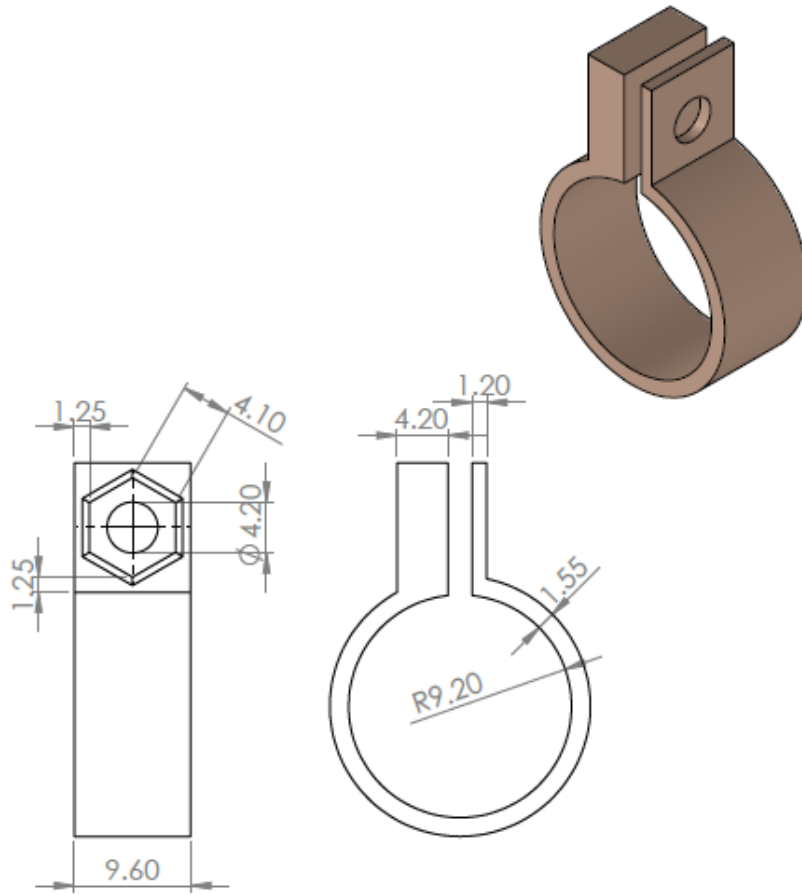
3D printer:	
Creality Ender 3	
Slicer:	
Ultimaker Cura 4.8.0	
Print setting	
Temperature	195°C
Layer height	0.2 mm
Print speed	50.0 mm/s
Support	None
Build plate Adhesion	Brim

ROUGHNESS:	FINISH:	MATERIAL: PLA (Jupiter serie; 123-3D.nl)	MASS [g]:
<small>THIRD ANGLE PROJECTION</small> 	SCALE: 2:1	DRAWN AND DESIGNED BY: NAME: Fatih Semih Yikilmaz STUDENT NUMBER: 4373634 E-MAIL: F.S.Yikilmaz@student.tudelft.nl	
	DIMENSION: mm		
	DATE: 31-03-2021		
	Biomechanical Engineering (BME)	NAME/DESCRIPTION: Syringe plunger joint (female)	A4



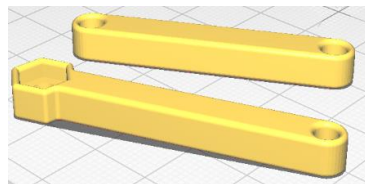
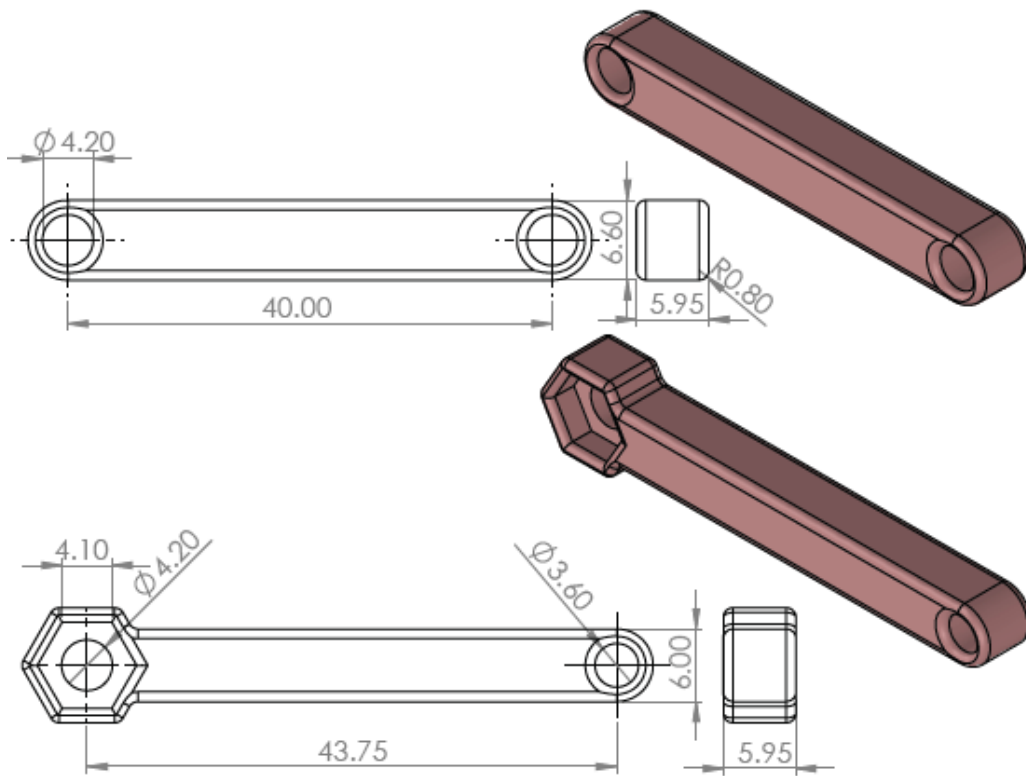
3D printer:	
Creality Ender 3	
Slicer:	
Ultimaker Cura 4.8.0	
Print setting	
Temperature	195°C
Layer height	0.2 mm
Print speed	50.0 mm/s
Support	None
Build plate	Brim
Adhesion	

ROUGHNESS:	FINISH:	MATERIAL: PLA (Jupiter serie; 123-3D.nl)	MASS [g]:
THIRD ANGLE PROJECTION 	SCALE: 2:1	DRAWN AND DESIGNED BY: NAME: Fatih Semih Yikilmaz STUDENT NUMBER: 4373634 E-MAIL: F.S.Yikilmaz@student.tudelft.nl	
	DIMENSION: mm		
	DATE: 31-03-2021		
	Biomechanical Engineering (BME)	NAME/DESCRIPTION: Syringe plunger Joint (male)	A4



3D printer:	
Creality Ender 3	
Slicer:	
Ultimaker Cura 4.8.0	
Print setting	
Temperature	195°C
Layer height	0.2 mm
Print speed	50.0 mm/s
Support	None
Build plate	Brim
Adhesion	

ROUGHNESS:	FINISH:	MATERIAL: PLA (Jupiter serie; 123-3D.nl)	MASS [g]:
THIRD ANGLE PROJECTION 	SCALE: 2:1	DRAWN AND DESIGNED BY: NAME: Fatih Semih Yikilmaz STUDENT NUMBER: 4373634 E-MAIL: F.S.Yikilmaz@student.tudelft.nl	
	DIMENSION: mm		
	DATE: 31-03-2021		
	Biomechanical Engineering (BME)	NAME/DESCRIPTION: Syringe chamber clamp	A4



3D printer:	
Creality Ender 3	
Slicer:	
Ultimaker Cura 4.8.0	
Print setting	
Temperature	195°C
Layer height	0.2 mm
Print speed	50.0 mm/s
Support	None
Build plate	Brim
Adhesion	

ROUGHNESS:	FINISH:	MATERIAL: PLA (Jupiter serie; 123-3D.nl)	MASS [g]:
<small>THIRD ANGLE PROJECTION</small> 	SCALE: 2:1	DRAWN AND DESIGNED BY: NAME: Fatih Semih Yikilmaz STUDENT NUMBER: 4373634 E-MAIL: F.S.Yikilmaz@student.tudelft.nl	
	DIMENSION: mm		
	DATE: 31-03-2021		
	Biomechanical Engineering (BME)	NAME/DESCRIPTION: Syringe crank and link	A4

B. Prototype pictures

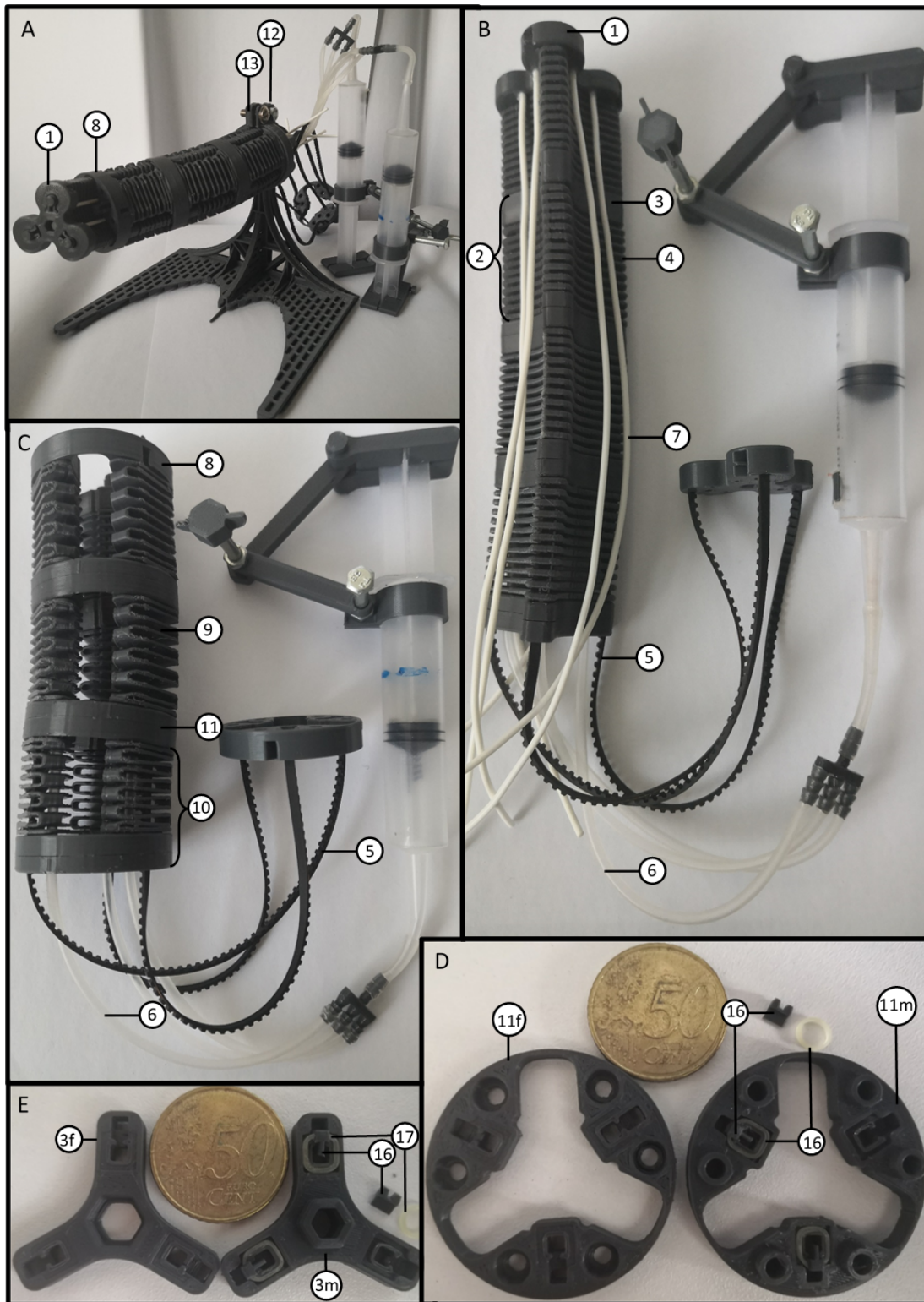


Fig. 26: **Pictures of the prototype parts before and after assembly.** (A) The full assembly of both inner- and outer-shaft concentrically positioned and attached to their stands (12 and 13). (B) The assembled inner-shaft consisting of four segments (2). The segments have a disk (3) and joint (4) that contain channels for the timing belts (5) and air tubes (6). The timing belts, air tubes and guiding wires (7) are attached to the end-effector disk (1). (C) The assembled outer-shaft consisting of three segments (10) containing a disk (11) and joint (9). The end-effector disk (8) fixes the air tubes and timing belts. (D) The female (11f) and male (11m) part of the outer-shaft disk (11). The disk chambers three stoppers (16) wrapped with elastic bands (17). (E) The female (3f) and male (3m) part of the inner-shaft disk (3).

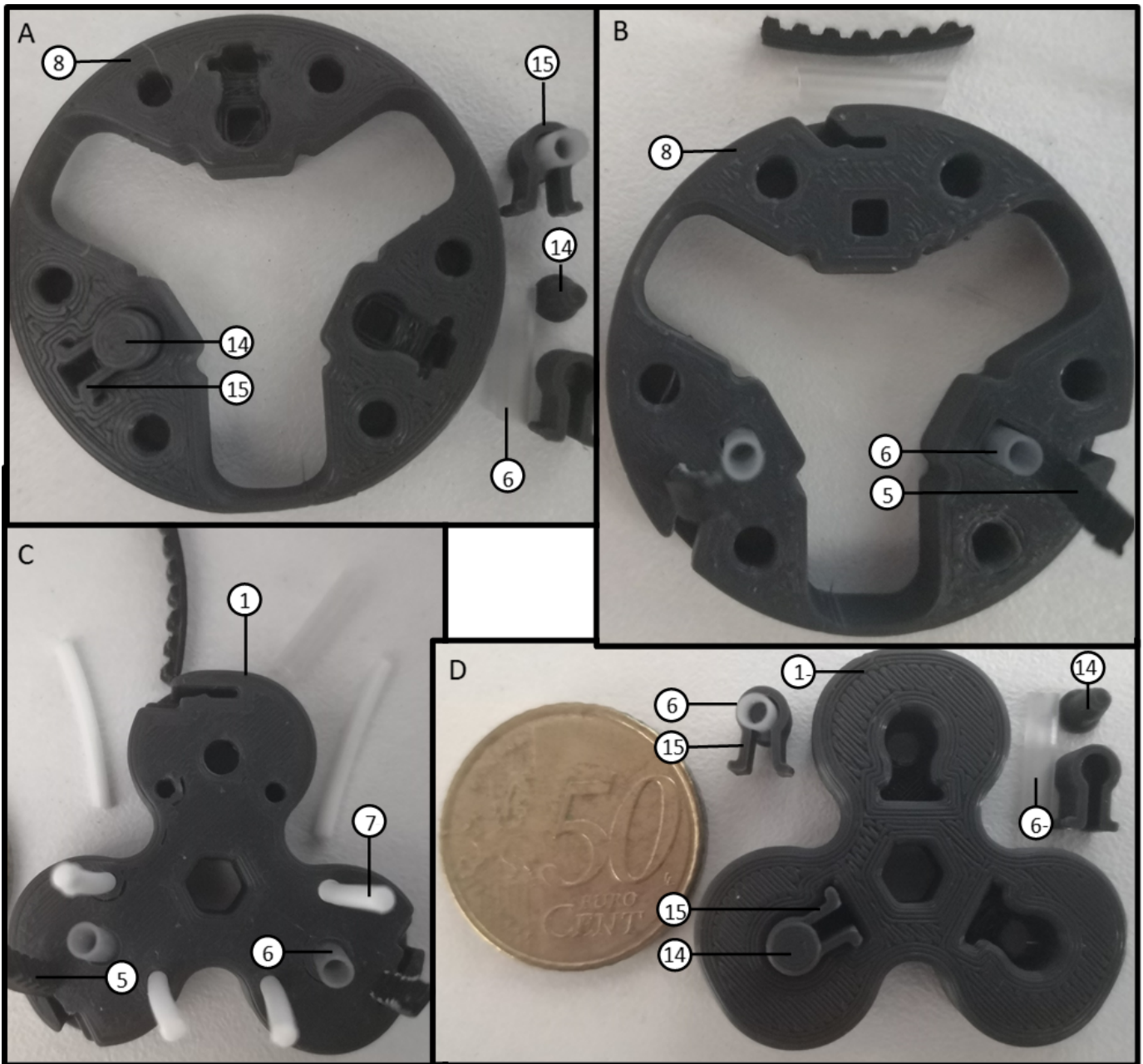


Fig. 27: **Pictures of the end-effector disks.** (A) The front side of the outer-shaft end-effector disk (8) contains slots to secure the silicone air tubes (6). The tubes are plugged (14) and clamped (15). (B) The back side of the end-effector disk contains slots to fix the timing belts (6). (C) The back side of the inner-shaft end-effector disk contains slots to fix the timing belts and guiding wires (7). (D) The front side of the end-effector disk contains slot to secure the silicone air tubes.

C. Part replacement demonstration

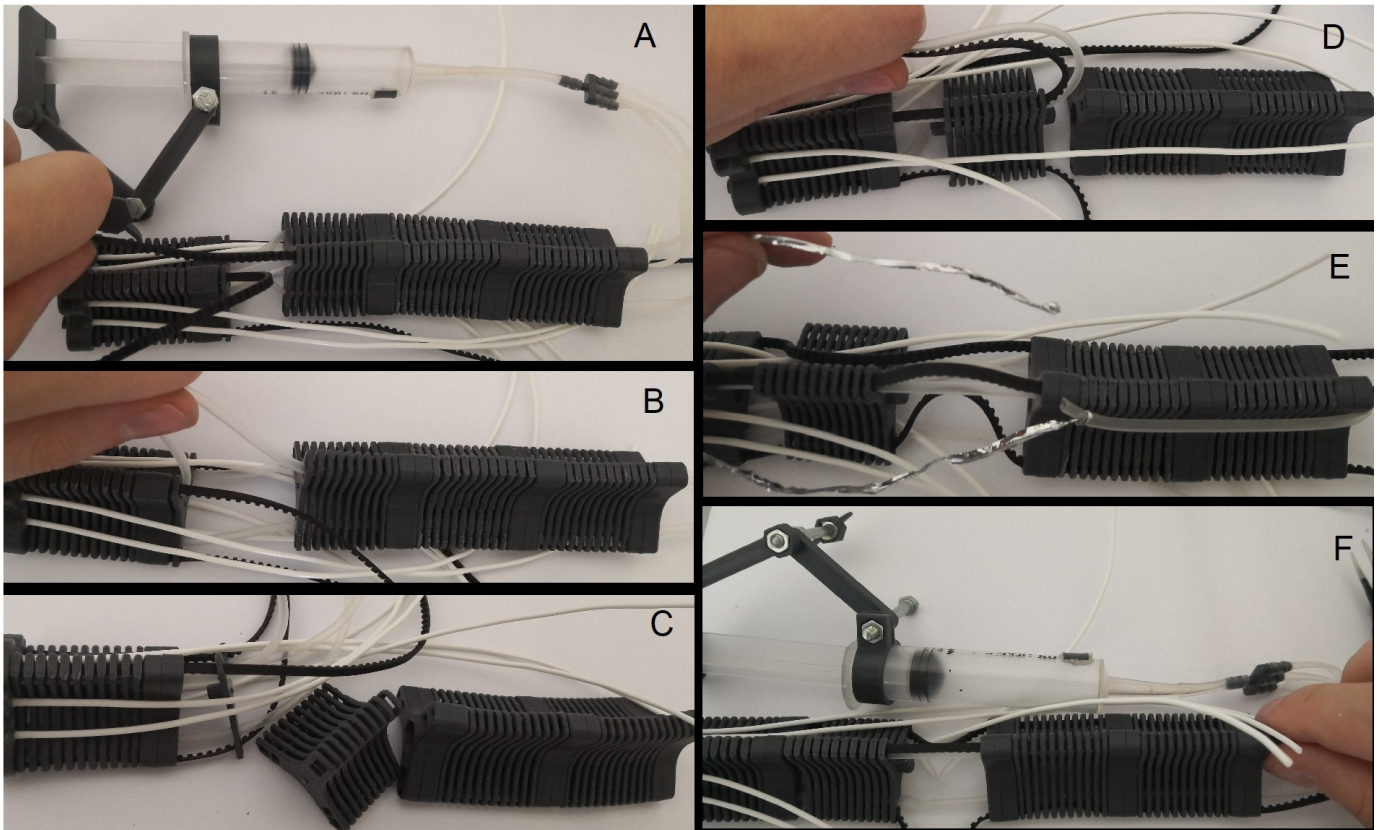


Fig. 28: **Step by step replacement of a segment joint.** (A) The air tubes are collapsed to allow for the timing belts to be removed. (B) The syringe is detached and the air tubes are pulled out. (C) The broken joint is removed. (D) First the timing belts and then air tubes are pulled through the replacement joint and the intact shaft. (E) To pull the air tubes a metal thread is used. (F) The air tubes are collapsed and the segments are moved towards each other by pulling the timing belts and the air tubes.